STUDIES ON INFLUENCE OF NANOPARTICLE CAPPING AGENT ON THE RESPONSE OF PALLADIUM BASED RESISTIVE HYDROGEN SENSORS

Thesis submitted in fulfillment of the requirements for the Degree of

DOCTOR OF PHILOSOPHY

IN

PHYSICS & MATERIALS SCIENCE

BY

POOJA

Enrollment No. 166901

Under the supervision of
Dr. P.B. Barman and Dr. S.K. Hazra
Department of Physics and Materials Science

Jaypee University of Information Technology
Waknaghat, Solan-173 234, Himachal Pradesh, INDIA

December 2021

JAYPEE UNIVERSITY OF INFORMATION TECHNOLOGY
(Established by H.P. State Legislative vide Act No. 14 of 2002)
Waknaghat, P.O. Dumehar Bani, Kandaghat, Distt. Solan – 173234 (H.P.) INDIA
Website: www.juit.ac.in
Phone No. (91) 07192-257999 (30 Lines)
Fax: (91) 01792 245362

Declaration

I hereby declare that the work reported in the Ph.D. thesis entitled "Studies on influence of nanoparticle capping agent on the response of palladium based resistive hydrogen sensors" submitted at Jaypee University of Information Technology, Waknaghat, India is an authentic record of my work carried out under the supervision of Dr. P.B. Barman and Dr. S.K. Hazra. I have not submitted this work elsewhere for any other degree or diploma. I am fully responsible for the contents of my Ph.D. Theses.

Signature:

_____

Date:

_____

JAYPEE UNIVERSITY OF INFORMATION TECHNOLOGY
(Established by H.P. State Legislative vide Act No. 14 of 2002)
Waknaghat, P.O. Dumehar Bani, Kandaghat, Distt. Solan – 173234 (H.P.) INDIA
Website: www.juit.ac.in
Phone No. (91) 07192-257999 (30 Lines)
Fax: (91) 01792 245362

Certificate

This is to certify that the work reported in the Ph.D. thesis entitled **STUDIES ON INFLUENCE OF NANOPARTICLE CAPPING AGENT ON THE RESPONSE OF PALLADIUM BASED RESISTIVE HYDROGEN SENSORS** submitted by **Pooja** at **Jaypee University of Information Technology**, is a bonafide record of her original work carried out under my supervision. This work has not been submitted elsewhere for any other degree or diploma.

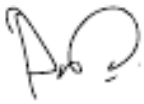

Signature of Supervisor-1:
Dr. P.B. Barman

Signature of Supervisor-2:
Dr.S.K. Hazra

Dedicated to My Beloved Master & Family.. . .

Acknowledgements

I thank the almighty God for letting me through all the difficulties and help me to finish this thesis work. It is my privilege to take the opportunity to thank all the individuals who were with me to achieve this target. A number of experiences have been encountered in JUIT, and I would like to thank those dozens of remarkable individuals.

First, and for most, I would like to thank my supervisor and head of the department Prof. (Dr) P.B. Barman, under whose guidance, I have completed my Ph.D. work. He always treated me like his daughter. I always cherished favouritism as well as I also never missed the scolding of a father in his presence. He always makes me comfortable to talk. His presence in every departmental presentation gave moral support to me. Ever since he has supported me not only in research but also offers potential suggestions and motivation throughout the rough road of finishing this thesis. His strictness to keep me stay in the lab proved as a boon for me as this was so hard to make a continuous sitting practice while writing the thesis. Thus, from the early morning to till late night hours living in the lab made a connection and interest to finish this endeavour. I also thank him for supporting this research work financially through university funds. Words cannot express to thank him for spending lots of hours to re-evaluate my reports and thesis. I could not complete this work without his enormous support in many ways.

I am also thankful to Dr. S.K. Hazra, my co-supervisor, for his encouragement and support during this Ph.D. journey. I remember, he always used to say that "I taught you to do small things carefully in a systematic way". Indirectly he always encourages me to move ahead. He tried to make me a hardworking person.When the experimental results in the lab were not satisfactory then instead of scolding me, he always appreciated my efforts. He made me understand to have patience during experimentation and taught me to do constant hard work to achieve the objectives of the research. His endless efforts and attention toward my work pushed me ahead to finish this research work. No expression of thanks will be sufficient for his enormous patience while reading my thesis. I have learned to do work systematically from him. He always made a balance of constructive criticism and praise so that I could not demoralize on any step. During the most challenging time when I was starting to write my thesis, he gave me the freedom to move on and provided constant help to complete my thesis work and made this a successful venture.

I owe my sincere thanks to the worthy administration department of JUIT, Prof (Dr) Vinod Kumar (Vice-Chancellor), Prof (Dr) Sameer Dev Gupta (Dean A & R), and Maj Gen Rakesh Bassi (Retd.) (Registrar) for providing financial support, laboratory facilities and necessary permissions to pursue Ph.D research work.

I want to thank the committee members, Prof (Dr) Sunil Khah, Dr Pankaj Sharma, Dr Rajesh Kumar, Prof (Dr) Vivek Sehgal, whose comments and feedback helped me a lot to improve my research work.

I would like to thank all the faculty members of Physics and Materials Science, Dr Sanjeev Tiwari, Dr. Vineet Sharma, Dr. Dheeraj Sharma, Dr. Ragini Raj Singh for their valuable support and suggestions throughout my work.

A special thank to Dr Anil, Dr Aman deep Acharya, Dr Kanchan, Dr Harjinder (Govt. College, Ldh), Dr Kavita Sharma, Dr Vandana Thakur, Dr Neha Kondal, Dr Sampan Attri, Dr Arun Sharma, Dr Ambika, Dr. Prabhat, Dr Prashant, Dr Rohit, Dr Jonny Dhiman, Dr Asha, Sonia ma'am (Bio lab), Dr. Deepika (Bio lab) for their incessant guidance and help, whenever I needed.

I emphatically extended my thanks to my friends and lab mates Sonu, Mahima, Kirti,

Nidhi, Dipti, Kanchan, Deepak, Priyanka, Neha, Prachi, Shivi, Jyotsna, Meghna, Shefali, Ayushi, Dhruv, Achyut Sir, Raj Sir, Shiv Sir, Rajan, Sanjay, Ekta, Shikha, Anuradha, Nadia, Monika for making stress relief environment around me.
I am highly obliged to lab staff members Mr. Pramod (ECE), Mr. Kamlesh Mishra (PMS), Mr. Ravendra Tiwari (PMS), Mr. Deepak Singh (PMS), for providing necessary assistance and lab facilities.
Special Acknowledgement: I want to pay heartfelt thanks to my parents for their sacrifices, prayers, and all-around support. To my beloved elder brother 'Jatinder' for encouraging me and always cheering me up throughout this journey. Thanks for your motivational speeches, my hero! At last, I would like to thank beloved God for showering blessings and holding me in every difficult situation. I experience your grace and guidance every moment of my life. You are the one who is always with me in every good and bad experience of my life. Ever since I have no words to thank you for whatever you have done for me. Thanks for guiding and being with me always. Thank you, lord.. . .

Pooja

Abstract

Palladium NPs were synthesized by the polyol reduction technique. These NPs have been studied for hydrogen gas sensing. The stabilizer [Polyvinyl pyrrolidone (PVP)] concentration, which is a synthesis parameter, was optimized with respect to the hydrogen gas response. It has been verified that the sensing performance was tuned by modifying this synthesis parameters. This is due to the shape and size attributes of nanoparticles which are function of this synthesis parameter. In this work, efforts have been made to correlate hydrogen gas sensing with PVP concentration (the chosen synthesis parameter). Nano palladium was characterized by HRTEM, GIXRD, and UV-Vis spectroscopy. Typical sensing mechanisms were formulated to visualize the sensing phenomenon.

HRTEM study showed that the palladium nanoparticle shape and size were dependent on stabilizer PVP. Different shapes *viz.*, nearly spherical, octahedron, etc., were obtained in this study. Hydrogen response pattern of these NPs near room temperature were correlated to the variation of the concentration of PVP. It was observed that the size distribution in palladium nanoparticle influenced the hydrogen sensitivity. The sensing was analysed with respect to the variation of NP size and size dispersity. The size modulation by PVP was verified by UV-Vis data where peak shift was observed with the increase in PVP. The H_2 response at elevated temperature was also studied.

Parametric study based on washing of NPs was done for understanding hydrogen gas sensor performance. It has been found that water washed palladium nanoparticles showed intense hydrogen response than ethanol washed nanoparticles. The strain data (from GIXRD) revealed that the water washed devices have more strain in the Pd atoms than ethanol washed Pd NPs; such difference in strain may assist the geometric response during hydrogen sensing. The negligible catalytic contamination of the sensing material was analyzed with XRD data. Furthermore, long term validity was proved by testing the devices for a period of 8-9 days regularly. In fact, reproducible behaviour was observed after one month of testing.

Publications

Journal Publications

- Pooja, P.B. Barman, & S.K. Hazra, Role of Capping Agent in Palladium Nanoparticle Based Hydrogen Sensor. J Clust Sci 29, 1209–1216 (2018).
- Pooja Bhardwaj, P.B. Barman, & S.K. Hazra, Effect of Capping-Agent Concentration on Size and Size Dispersity of Palladium Nanoparticles for Resistive-Type Hydrogen Sensors. J Electron Mater 49, 6656–6670 (2020).
- Pooja Bhardwaj, Partha Bir Barman, and Surajit Kumar Hazra, "Hydrogen response of palladium nanoparticles washed with different solvents", Bull Mater Sci 44, 45 (2021).

Conference Publications

- Pooja Bhardwaj, Partha Bir Barman, and Surajit Kumar Hazra. "Shape dependent hydrogen response in palladium nanoparticle based sensors", Materials Today: Proceedings 28(1), 218 (2020).
- Pooja, P.B. Barman S.K. Hazra "Sensing mechanism of resistive palladium nanoparticle based hydrogen sensors", Rural Upliftment Through Science & Technology, pp.170(2018). Abstract published in 3rd Himachal Pradesh Science Congress Conference at IIT mandi during 22-23th October 2018 entitled Rural Upliftment Through Science & Technology Interventions

Workshop

- Attended Workshop on "Material Characterization Techniques" (May 20-24, 2019) (Sponsored by TEQIP-III) jointly organized by Dr B.R. Ambedkar National Institute of Technology (NIT), Jalandhar, Punjab.

Contents

List of Figures

List of Tables

List of Abbreviations

NP	**N**ano **P**article
NPs	**N**ano **P**articles
Pd	**P**alladium
PPM	**P**arts **P**er **M**illion
GIXRD	**G**lancing **I**ncidence **X** **R**ay **D**iffraction
HRTEM	**H**igh **R**esolution **T**ransmission **E**lectron **M**icroscopy
UV-vis	**U**ltra **V**iolet **v**isible **spectroscopy**
PVP	**P**oly **V**inyl **P**yrrolidone
H_2	**H**ydrogen
Pd	**P**alladium
Mw	**M**olecular **w**eight
XRD	**X** **R**ay **D**iffraction
SAED	**S**elected **A**rea **E**lectron **D**iffraction
nm	**n**ono **m**eter
ppm	**p**arts **p**er **m**illion
W-H	**W**illiamson-**H**all
RT	**R**oom-**T**emperature
S/V	**S**urface/**V**olume
DMM	**D**igital **M**ulti **M**eter
FWHM	**F**ull **W**idth at **H**alf **M**aximum
JCPDS	**J**oint **C**ommittee of **P**owder **D**iffraction **S**tandards
SPR	**S**urface **P**lasmon **R**esonance
kohm	**k**ilo **ohm**
PDI	**P**oly **D**ispersity **I**ndex
FCC	**F**ace **C**entred **C**ubic

Chapter 1

Introduction

1.1

Detection and sensing of things are the essential requirements of daily life. A sensor is a device which detects the presence of a living or non-living matter in the surrounding. A sensor senses a physical stimulus (heat, light, smell, sound) and responds to it in a particular way. Sensors can be classified as natural and artificial sensors (human-made sensors). A human body includes various natural sensors like eyes, nose, tongue, skin for the purpose of seeing this world, to smell flowers, to taste the sweets, and to feel the environment respectively [26]. Artificial sensors are man-made sensors which can sense as well as to measure the changes to the reaction. For example, a temperature sensor responds to heat as well as measures the temperature of the object. In other words, the sensor is a device which captures physical, chemical, optical events and gives the results to the electronic devices for processing the output signals.

A **chemical sensor** is a sensing device which transforms the chemical information (such as availability of particular chemical, *etc.*) into useful analytical signals. The phenomenon like adsorption, solid-gas interaction, ion exchange reaction, and molecular recognition are considered as the working principles for these types of sensors.

A **gas sensor** is a type of the chemical sensor which works on the principle of solid-gas interaction. Gas sensing has become indispensable in this modern world for environmental protection and safety purposes. Some gases are vital to life while many others are hazardous to human health. Useful gases such as oxygen (O_2) must be maintained to an adequate level while some unsafe industrial waste gases like carbon monoxide (CO), hydrogen (H_2), sulfurized gases (H_2S, SO_2) must be controlled before crossing the danger level. In order to achieve this target, it is necessary to study the various aspects of gas sensors.

Resistive gas sensors are very commonly used devices, in which electrical resistance of the sensing material changes markedly on the adsorption of gas. Detection is accomplished by monitoring the increase/decrease in electrical resistance occurring due to absorption of test gas. The resistance change of a sensing device mainly depends upon the concentration of the test gas.
Sensors characteristics can be broadly classified with the following parameters:
%response indicates the percentage change in sensor's output for a certain concentration of test gas. Mathematically it is expressed as.

$$\%\text{response} = \frac{\text{Change in signal}}{\text{Initial value of the signal}} \times 100 \tag{1.1}$$

For resistive gas sensors with initial baseline resistance R and change in resistance ΔR incurred upon exposure to a certain concentration of test gas,

$$\%\text{response} = \frac{\Delta\, R}{R} \times 100 \tag{1.2}$$

"Response time": It is the time required by a sensor to rise by 90% of its maximum signal strength after exposing the sensor to a particular gas concentration. For resistive H_2 sensors with initial baseline resistance R and change in resistance ΔR incurred upon exposure to a certain concentration of H_2, the "response time" is the time necessary to attain a resistance of magnitude $(R \pm 0.9\ \Delta R)$.
Recovery time: The time necessary for a sensing device to return to the starting resistance from its saturation value by 90% after cutting off the test gas supply. For resistive gas sensors with initial baseline resistance R and change in resistance ΔR incurred upon exposure to a certain concentration of test gas, the "recovery time" is the time taken by the sensor to reach a resistance of magnitude $[(R \pm \Delta R) \mp 0.9\Delta R] = (R \pm 0.1\Delta R)$ after signal saturation.
Selectivity: Ability of a gas sensor to detect some components in an unknown gas mixture is called the selectivity of the sensor [21].

1.2 RESISTIVE HYDROGEN GAS SENSORS

Hydrogen is a highly explosive, colourless, odourless and tasteless gas. Therefore, human senses cannot recognize its presence and alternative techniques are required

to recognize its presence and concentration in the ambient air. Fast and precise hydrogen gas detection is possible with sensors in order to avoid the danger of explosion [36]. Since hydrogen is being used extensively by several industries for versatile applications (like plastic recycling, methanol production, compost making, *etc.* [73]), it is necessary to cultivate more on device parameters that control the performance of hydrogen sensors. Moreover, hydrogen sensors are significant because hydrogen gas is an important fuel in industry. There are an enormous number of sensors developed so far, for hydrogen detection [27, 43, 64, 69]; however, the role of nano-palladium (Pd-NP) synthesis parameters have not been explored much for the development of robust resistive hydrogen sensors. In this work, an attempt has been made to correlate the synthesis aspects of nano palladium with the end performance of nano palladium based resistive hydrogen sensors.

Dealing with nanotechnology (nano-sensors): Nanomaterials have more prevalent properties than the bulk materials due to acquiring high surface to volume ratio (S/V) of nanoparticles which contributes good catalytic efficiency to the resultant material. S/V ratio can affect the relative sensitivity of the sensing material. Bulky sensing elements show low sensitivity towards gases due to small S/V ratio. The nanomaterials (having large S/V ratios) are superior to bulk materials due to their good catalytic properties, thermal stability, mechanical strength, and enhanced electric characteristics. Large S/V ratio also enhances the reactivity region of nanoparticles. Mathematically, S/V ratio is inversely proportional to the radius of a spherical nanoparticle $\Rightarrow \frac{S}{V} = \frac{4\pi r^2}{\frac{4}{3}\pi r^3} = \frac{3}{r}$. For bulk materials, r approaches to infinity. Therefore, $\frac{S}{V} \rightarrow 0$. For nano field, 'r' has small magnitude (and not equal to zero), so $\frac{S}{V} \rightarrow \infty$. So the ultimate goal is to maximize the S/V ratio in order to amplify the catalytic nature of nanoparticles [31].

1.3 CHOICE OF SENSING MATERIAL

Various nanoparticles have been used for the hydrogen gas sensor application [14, 15, 28, 41–43, 51, 65, 70, 96]. Normally metallic nanoparticles are chosen for gas sensing studies. They are mainly preferred for their good properties such as having good conductivity and optical effects. They can be easily capped by the external molecular ligands, e.g., polymers (Polyvinylpyrrolidone), which enhances the resultant characteristics of nanocrystals [21]. It is easy to vary the size and shapes of

these materials which enhances the S/V (surface to volume) ratio of nanoparticles. Nanoparticles acquire large surface energies because of high S/V proportions at the nanoscale system. Subsequently, nanoparticles have a firm tendency to form into spherical or nearly spherical nanostructures to limit the surface energy [98]. Therefore, large S/V of material is essential for stable nanoparticles and to minimize its surface energy [9].

Palladium (Pd) nanoparticles have been the best sensing material for hydrogen detection due to its strong affinity towards hydrogen atoms. Pd nanoparticles are normally used as catalyst in many chemical reactions specifically for hydrogenation such as Mizoroki-Heck and "Suzuki-Miyaura cross-coupling reactions" [39], oxidation of alcohols [45], Olefin hydrogenation [49], Suzuki coupling response[49], Allylic alkylation [40], alkene hydrogenation [52], cross-coupling of aryl halide and tin amides [68], carbon cross-coupling [78], catalyst in Heck's Reaction [10] and many more.

1.4 ROLE OF CAPPING AGENT

Capping agent (stabilizer) is a polymer or a surfactant which is used to coat the nanoparticles. It controls the size as well as prevents the agglomeration of nanoparticles. Moreover, the final morphology of the nanoparticles also depends upon the amount of capping material used, which profoundly affects the results. Polyvinyl pyrrolidone is commonly used stabilizer in the generation of Pd NPs. The surface coverage of this polymer on the palladium nanoparticles can tune the interparticle barrier between two palladium nanoparticles. Such a barrier tuning can affect the gas sensor characteristics of this nanoparticle.

The role of PVP in size control of nanoparticles helps to enhance their gas sensor performance. PVP capping and growth stabilization attributes also help in the evolution of various new shapes. Capping also controls the size dispersity of nanoparticles. Thus, the sensing performance can be influenced by size and shape factors [61]. Based on all these multiple benefits such as controlling growth, preventing agglomeration, uniformity of shape, size, *etc.*, an idea of choosing this capping material for improvement in gas sensing ability of palladium nanoparticles has been considered.

1.5 SOLID-GAS INTERACTION (PALLADIUM HYDROGEN SYSTEM)

Solid palladium nanoparticles interact with hydrogen gas on the particle surface in the hydrogen atmosphere. The H-Pd (hydrogen-palladium) association results in the formation of "palladium hydride (PdH_y)" [Figure 1.1]. It is reported that binding energy (B.E.) for PdH_y bonding is 2.34 eV [56]. For y<0.015, the "α-phase of palladium hydride" is predominant, and the transformation to the "β-phase" happens in the range "0.015<y<0.7" [53]. "β-phase of the palladium hydride" is an undesirable state of sensing in which Pd atoms are unable to release the adsorbed hydrogen in order to regain pure metallic state. This is sometimes termed as catalytic poisoning of Pd nanoparticles which reduces the adsorption efficiency of these nanoparticles. Several reports give an account of the interaction between hydrogen and Pd nanoparticles in order to justify different hydrogen sensing mechanisms; for instance, increment in resistivity of metallic palladium and volumetric expansion of palladium lattice after hydrogen adsorption [28, 46] are interesting solid-gas phenomena. In fact both these happen sequentially, when palladium nanoparticles are exposed to hydrogen[28].

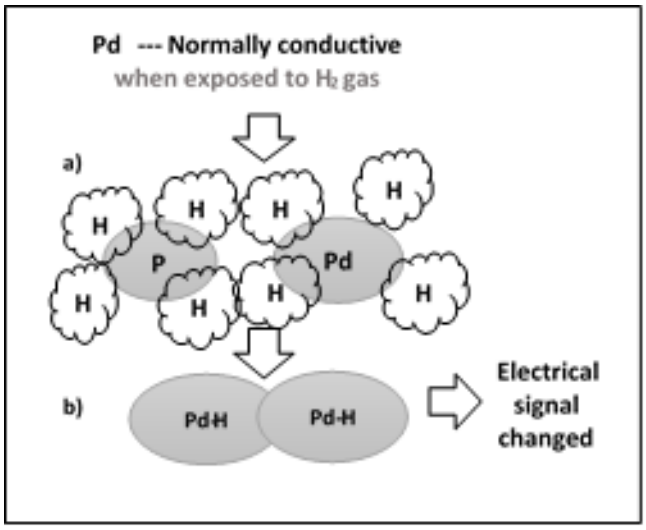

FIGURE 1.1: Pd sensing mechanism a) Pd exposed with hydrogen gas b) swelling of Pd atoms

1.6 WORKING OF PALLADIUM NANOPARTICLE BASED RESISTIVE SENSOR IN HYDROGEN AMBIENT

Pure palladium nanoparticle based hydrogen sensors normally manifest electronic and geometric response patterns. These effects are due to the interaction of palladium with hydrogen. Depending on the available interparticle barrier, response will be either electronic or electronic & geometric. The response(s) will be followed by recovery. The cause of electronic & geometric responses are the increase in resistivity of the palladium nanoparticles and the subsequent change in nanoparticle volume upon hydrogen adsorption. However, only electronic effect will be observed in the response pattern if the interparticle gap/barrier is negligible. In case there is sufficient interparticle gap/barrier, both electronic & geometric effects will be observed. The interparticle gap/barrier can be due to many reasons, and one important factor that can tune this gap/barrier is the presence of a polymeric stabilizer, which is used during the synthesis of palladium nanoparticles. During electronic effect, only the sensor device resistance increases due to the generation of PdH_y whose resistivity is relatively higher with respect to palladium. This electronic effect is normally followed by the geometric effect during which the palladium nanoparticles increase their volume and in the process reduce the interparticle gap/barrier. So the sensor device resistance decreases during geometric effect. A schematic diagram is presented in Figure 1.2 for these effects.

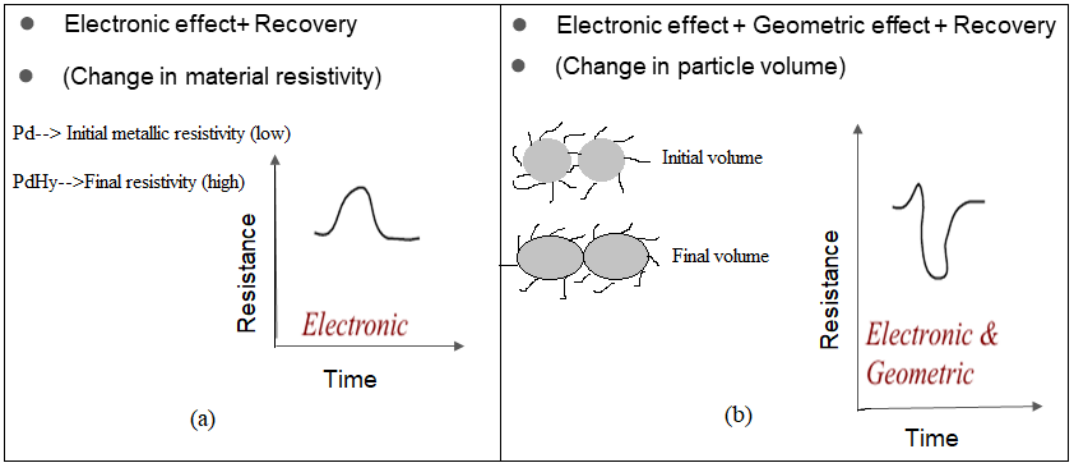

FIGURE 1.2: (a) Electronic effect followed by recovery and (b) Electronic & Geometric effects followed by recovery in sensor devices

1.7 THE MOTIVATION BEHIND THE THESIS

The work was taken up to explore the mutual dependency of synthesis parameter (of nano palladium) and the corresponding room temperature hydrogen response in resistive devices. If the synthesis parameter is varied, the nano palladium yield will change and accordingly the gas adsorption characteristics will change. The parametric research was focussed on one synthesis parameter (the capping agent concentration) variation to bring change in nanoparticle morphology such as change in size, shape, *etc.* Such variation in particle attributes will also alter their ensuing catalytic activity [55, 58]. The capping agent concentration was further controlled after synthesis by washing the nanoparticles in different solvents. Basically some solvents have the ability to attack the capping layer on the nanoparticle surface. Numerous research works have been accomplished regarding palladium (Pd) hydrogen gas sensing. However, the parametric control with respect to the capping agent (stabilizer) variation was a lacunae that motivated the current research work.

1.8 THE FRAME OF THE THESIS WORK

The study was conducted with the following objectives:

- To fabricate resistive hydrogen sensors with palladium nanoparticles synthesized by incorporating the following variations:
  - Change of stabilizer (Mw 8000) concentration (in synthesis) to bring change in palladium nanoparticle shape and size.
  - Tuning the stabilizer coverage (Mw 8000) on nanoparticle surface after synthesis to bring change in palladium nanoparticle activity.
  - Increase the stabilizer molecular weight (Mw 40000) to bring change in interparticle barrier.
- To analyse the catalytic nanoparticle purity (extent of hydrogen contamination) and device stability.

All the above objectives were successfully accomplished and the thesis has been organized with the following chapters:

- Chapter 1: Introduction.

- Chapter 2: Experimental
- Chapter 3: Effect of shape/size of palladium nanoparticles on the hydrogen response.
- Chapter 4: Role of stabilizer (Mw 8000) coverage on nanoparticle surface on the hydrogen-palladium nanoparticle activity.
- Chapter 5: Influence of stabilizer molecular weight on inter-nanoparticle surface barriers and the hydrogen response pattern of resistive hydrogen sensors.
- Chapter 6: Catalytic nanoparticle purity (extent of hydrogen contamination) and resistive device stability.
- Chapter 7: Summary and conclusion

Chapter 2

Experimental

Chemical synthesis of metallic nanocrystals involves the reduction of metallic precursors followed by nucleation and growth of the generated species. A synthesis technique becomes exciting and novel if the synthesis parameters can be precisely optimized. Optimization of synthesis parameters refers to finding out the best suitable set of conditions or environment to achieve the desired yield. It is an essential step before undergoing synthesis of nanoparticles to guess the starting magnitudes of the parameters. Once the parametric survey (with the help of available literature) has been done, it becomes easy to start the synthesis and the subsequent optimization.

Preparation techniques also decide the catalytic efficiency of prepared NPs [32]. Properties of the end product profoundly depend on the synthesis strategy. The catalytic efficiency of nanoparticles relies on the size and shape of the resultant NPs, which depends on the chemistry of nanoparticles. The interdependence of synthesis (or synthesis parameters) on the properties of palladium nanoparticles is presented in Figure 2.1.

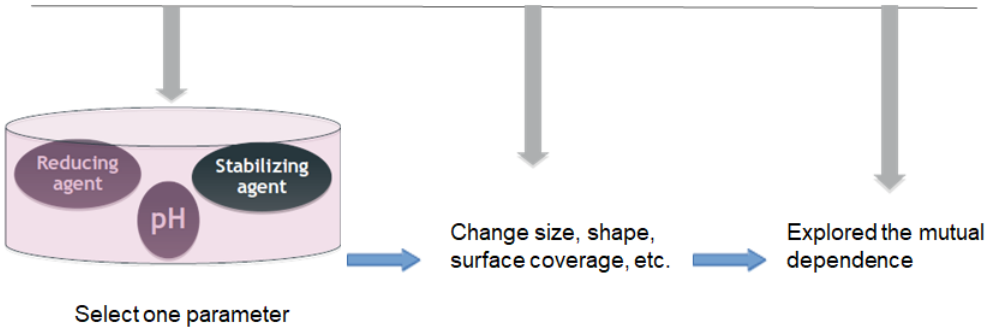

FIGURE 2.1: Synthesis yield characteristic interdependence

Herein the word "parameter" deals with variables and constants of the synthesis

such as ingredients, reaction time, temperature, stirring velocity, *etc.* The parametric research between the characteristics (size, shape, *etc.*) of NPs and their ensuing catalytic activity [55, 58] has generated interest to strengthen the hydrogen gas sensor application. For instance, the size of the nanoparticles relies on the synthesis strategy and its parameters. The size-specific Pd NPs were examined on a large scale to improve their catalytic activity [74]. In addition, morphological investigation of NPs is one of the best approaches to understand the catalytic activity of nanoparticles. Many reports have been published on the shapes and catalytic activity of the NPs; however, the connection between both is often not clearly correlated [12, 16, 24, 59, 60, 77, 99]. The experimental parameter (concentration of PVP) is varied in this work to explore the impact on nanoparticle morphology and the hydrogen response. Furthermore, the choice of washing agent (which is an experimental parameter) and the subsequent impact of washing on the PVP coverage around the nanoparticle surface is also verified experimentally. This in turn establishes the role of washing agent on the gas adsorption/desorption efficiency of catalytic palladium nanoparticles. In this study, the following experimental works were performed: (i) **Synthesis** of monometallic (Pd) nanoparticles by parametric control (ii) **Characterization** of synthesized material (iii) Hydrogen **sensor study**.

2.1 SYNTHESIS OF MONOMETALLIC (Pd) NANOPARTICLES BY PARAMETRIC CONTROL

There are broadly two ways to synthesize nanosized particles: (a) top-bottom and (b) bottom-up. The top (large) - bottom (small) approach starts with the bulk material, which breaks down into small particles by following a suitable technique. However, the bottom (small) - up (large) approach starts from the atoms/clusters/nuclei and forms the nanostructures by nucleation and growth of particles. The bottom-up approach is generally a wet chemical approach (e.g., reduction method, precipitation method), and top-bottom is the physical approach (lithography, etching, *etc.*) of synthesis. The bottom-up approach is considered less expensive and easy to conduct. A few of the chemical routes under bottom-up approach have been enlisted below:

- Reduction method
- Reverse micelle method

- Sol-gel method
- Co-precipitation Method.

The bottom-up approach, particularly the reduction method, has been chosen for Pd nanoparticle synthesis in this thesis work.

2.2 HIGHLIGHTS OF REDUCTION METHOD (POLYOL)

Polyol synthesis strategy is well-established for nanocrystals. Characteristics of nanoparticles such as size, shape, crystallinity can be easily tuned by this method. This synthesis strategy involves the reduction of the precursor by solvent (polyol) using a suitable stabilizing agent at an appropriate temperature. A series of work on polyol technique has started from 1989 by Fievet, Figlarz, and Lagier. The first synthesis by polyol strategy has been done on Co, Ni, Cu, and Pt particles [17, 18] then extended this plan to other elements, such as Re, Ru, Rh, Au, Sn. In 2000, fine particles of $Co_{20}Ni_{80}$, FeNi, Co_xCu_{1-x}, FeCoNi, *etc.*, were synthesized by polyol strategy for studying magnetic characteristics [88]. This synthesis strategy gathered attention because of precise size, shape, and crystallinity control [85, 91, 92]. It depends on several key parameters such as polyol, solvent, capping agent, precursor concentration, and reducing agent. The typical polyols are ethylene glycol, propylene glycol, and penta methylene glycol having viscosity (η) values η = 6.1, 40.4, and 140 mPa s, respectively. The viscosity values are based on the chain length of hydrocarbon (for polyols) [92]. The right selection of polyol affects the nucleation and subsequent growth of nanocrystals during reduction of metallic precursors [84, 94]. The reduction happens at high temperatures because polyols are converted into various aldehyde and ketone groups, and these enable the reduction of metal precursors.
The stabilizer is an essential component of synthesis for modulating size & shape of the nanocrystals. Polyvinylpyrrolidone (PVP) is a stabilizing agent in the polyol synthesis. PVP caps a metal nanocrystals (NCs) via adsorption on the nanocrystal surface. For this the carbonyl group of the pyrrolidone ring is very effective. [18, 44, 79, 81, 88, 92, 94].
The PVP-metal bond at specific crystal faces facilitates onsite reduction at some faces of the growing crystals. This enables anisotropic growth during synthesis. This mechanism can lead to the formation of metal nanocrystals with different facets. The mechanism of capping PVP on specific crystal facets is complicated and is still

under study. Furthermore, the reaction temperature, reactant amount, and reaction time have an appreciable effect on nanoyield size and morphology.

A successful polyol synthesis and the final yield of NPs relies on the different synthesis parameters, which include the ingredients of the reaction as well as the reaction conditions under process. Synthesis parameters of polyol techniques are: (a) Precursors (b) Solvent (c) Reducing agent (d) Capping agent (e) Reaction temperature (f) Reaction time (g) pH. Polyol is considered as a prime ingredient in the polyol method. It is used as a solvent as well as a reducing agent [19]. The reaction temperature can be raised up to the boiling point of polyol if the elements are not easily reduced at low temperature. This helps in the fast completion of the reaction. The end product obtained through polyol synthesis depends upon the stability of the resultant nanoparticles. Formation of nanoparticles mainly relies on the reduction process and the choice of reducing agent (polyol). Order of mixing of all ingredients also affects the results, because the chemical reaction may complete in any specific step during synthesis. Sometimes the reaction needs some additional base (NaOH) or acid (HCl) to finish the reduction. In some particular case, when polyol and acid/base combination seems insufficient to reduce the metal, an extra reducing agent and capping agent are also utilized (Figure 2.2).

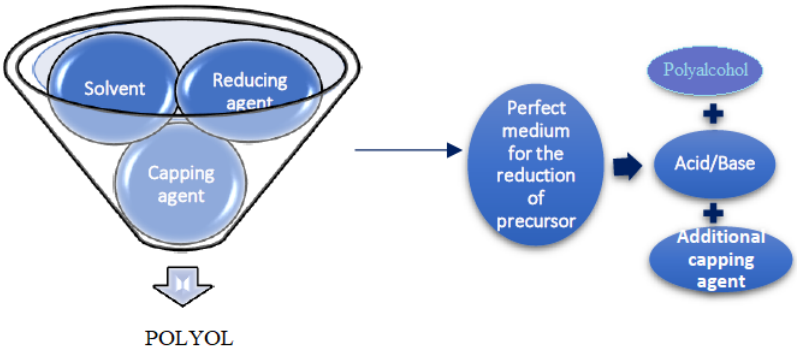

FIGURE 2.2: Polyol strategy showing its additional combinations (acid/base + capping agent) to reduce precursor completely.

2.3 POLYOL SYNTHESIS OF PALLADIUM NANOPARTICLES

The following materials were selected for the synthesis of palladium nanoparticles.

- Precursor:Sodium tetrachloropalladate (II) hydrate, ($Na_2PdCl_4.3H_2O$; 99.999% purity).
- Reducing agent: Ethylene glycol (99%)
- Capping agent: PVP (Polyvinyl pyrrolidone)
- pH controller: HCl (Hydrochloric acid) fuming 37%
- Washing solvent: Distilled water/ethanol

All the chemicals (high purity) have been purchased from Alfa Aesar & Merck. Monometallic Pd NPs were prepared by polyol technique. Ethylene glycol (from the polyol series) was used as the solvent and reducing agent for the palladium precursor ($Na_2PdCl_4.3H_2O$). The reaction temperature was approximately decided by considering the boiling point of ethylene glycol, which is $\sim 198^oC$. A moderate reaction temperature was chosen for this study i.e., 127 ($\pm$ 3)^{o}C due to two reasons: First, the synthesis was carried out at normal atmospheric pressure without using refluxing. Hence the temperature must be much lower than the boiling point in order to reduce the solvent loss by evaporation. Second, to avoid very fast reaction and subsequent particle agglomeration, relatively lower temperature is preferred. However, below 100^{o}C, significant precursor reduction was not observed. Small precursor quantity (51-mg $\pm$ 1-mg) was chosen because a little quantity of yield was necessary for sample characterization and preparation of sensor devices. Sufficient reaction time ($\sim$ 2-h) was given in order to ensure complete reduction of the precursor. The optimization was done with respect to the capping agent and the choice of washing agent as outlined below: The synthesis started with the addition of 0.051 g of palladium precursor ($Na_2PdCl_4.3H_2O$) in 10 ml of ethylene glycol in a 25 ml beaker at RT. Simultaneously a fixed quantity of PVP was added. The function of PVP is to act as the stabilizer/capping agent for the palladium nano yield. Normally polyol in presence of an additional acid acts as a good reducing agent. Therefore, six drops of HCl (for acidic pH control) were added. The reaction was carried out at 127($\pm$ 3)^{o}C on a hot plate. The reaction continued for a total time of 2-h. The colour changed from golden yellow (at 27^{o}C) to red-black (at elevated temperature). Finally, the colour became black with the progress in time. After completion of the reaction time, the solution was cooled back to 27^{o}C. After centrifugation at 5000 rpm, particles were extracted and washed with ethanol/distilled water. This drained out by-products

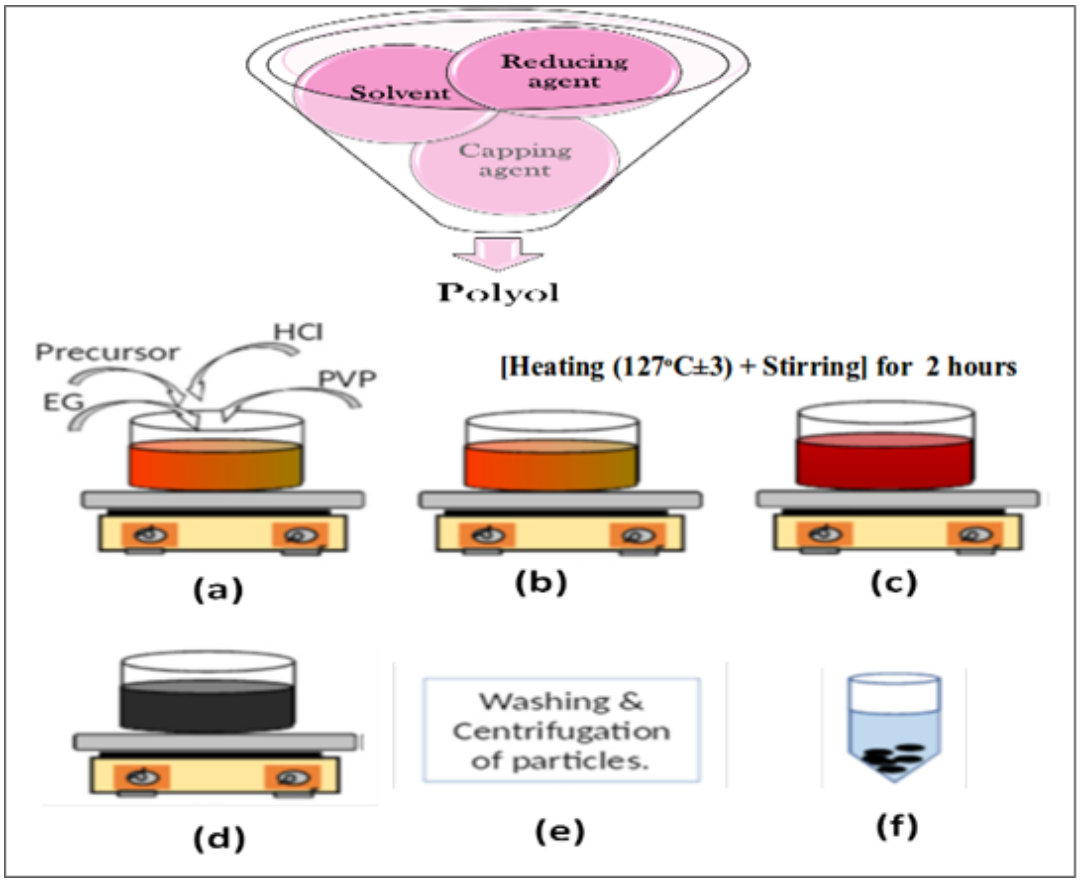

FIGURE 2.3: Schematic of the synthesis

and extra polyol. The steps are represented by a schematic (Figure 2.3).

The variations in the synthesis parameter (particularly capping agent and washing solvent) incorporated in the above procedure to synthesize different yields are tabulated in Table 2.1. The value of 'x' is ratio of the amounts of PVP and palladium precursor. Two molecular weights of PVP (8000 & 40000) and two washing solvents (ethanol & distilled water) were used. Reaction of Na_2PdCl_4 with Ethylene Glycol (EG) is shown in equation 2.1:

$$\begin{aligned} OHCH_2CH_2OH &\rightarrow CH_3CHO + H_2O \\ \text{Ethylene Glycol} &\rightarrow \text{Aldehyde} + \text{Water} \\ Na_2PdCl_4(aq.) + 2CH_3CHO &\rightarrow Pd\downarrow + 2NaCl + CH_3CO - OCH_3 + 2HCl \end{aligned} \tag{2.1}$$

2.4 CHARACTERIZATION OF SYNTHESIZED MATERIAL

Sample analysis was done by

- HRTEM (Tecnai G2 20 S-TWIN, FP 5022/22; FEI, USA)

TABLE 2.1: Synthesis parameter variation

PVP%	x=Ratio of PVP : Precursor	PVP molecular weight (Mw)	Washing solvent
0	0 : 1	—-	Ethanol
20	0.20 : 1	8000	
32	0.32 : 1		
45	0.45 : 1		
60	0.60 : 1		
20	0.20 : 1	8000	Ethanol
20	0.20 : 1		Distilled water
20	0.20 : 1	40000	Ethanol
32	0.32 : 1		

- UV-Vis (Perkin Elmer Lambda 750)
- GIXRD (Bruker D8 Advance).

HRTEM study was done to find out the size distribution of Pd NPs within the solution. In HRTEM, a beam of electrons passes through the specimen and the transmitted electron beam (dependent on the properties of material) is examined. The transmitted beam hits a phosphor screen.

For HRTEM, copper grids are used. Palladium nanoparticles are sonicated for the period of 30 min before use. This is necessary to avoid cluster formation in nanoparticles. Ultra-sonication disperses the nanoparticles thoroughly in the solution and remove agglomeration. Solution is taken out by a syringe or pipette out from the Eppendorf vessel. Thereafter, the solution is dispersed on a copper grid dropwise and allowed to dry for use. A schematic of all the steps which are being followed during sample preparation is shown is Figure 2.4. A UV-vis spectrophotometer is

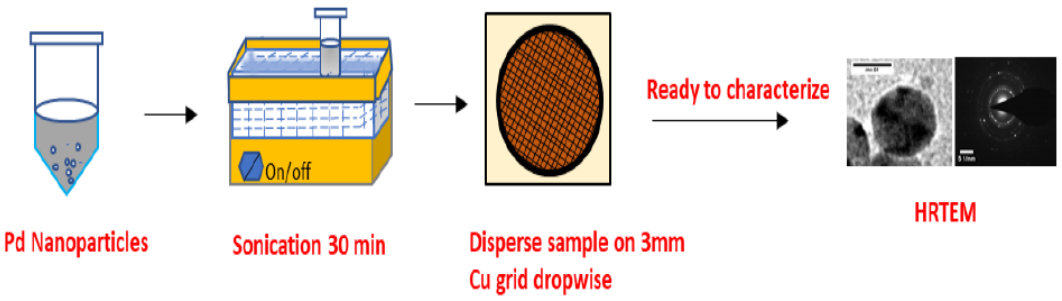

FIGURE 2.4: Schematic of HRTEM characterization.

used to perform absorption spectroscopy. The instrument operates by incidenting

a light beam and measuring the transmitted intensity with a detector. The beam of light can be considered as a current of photons. In this process, a photon induces an electronic transition. The optical energy in the form of ultraviolet or visible light excites electrons in the molecules/atoms to higher molecular orbitals, which results in an absorption spectrum.

The UV-Vis spectroscopy was performed by putting the sample in a quartz cuvette. The concentration of the solution is such that the absorbance is between 0.05 to 1.0 [2]. For this purpose, the solution has to be diluted with a reference solvent. The appearance of the solution must be near to a transparent form. A dense solution obstructs the light to a greater extent, which makes it unable to produce relevant results. Therefore, 0.05 ml of Pd solution was added to 2 ml of reference washing solvent. Then solution was shaken and sonicated for 15 minutes before performing the experiment for uniform dispersion of particles. Now, the solution was transferred to the cuvette to be used for UV-Vis analysis. Figure 2.5 clearly shows the steps which has been followed during UV-Vis spectroscopy study. For GIXRD mea-

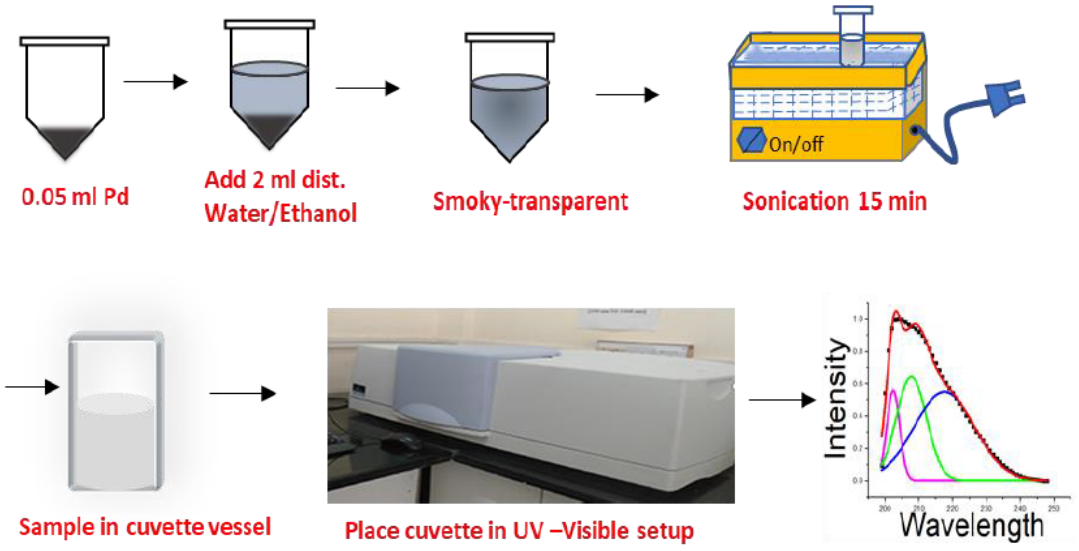

FIGURE 2.5: UV-Visible experiment set up mentioned with the steps to perform the experiment.

surements, palladium nanoparticle films were used. The sample film was developed by drying a drop of particle-washing agent solution on substrates (glass coverslips). The surface of substrates (size 8 mm square) was made rough by scrating with a diamond pen. Approximately 0.05 ml solution was used to put two drops on the cleaned roughened glass surface and subsequently dried on a hot plate. Figure 2.6

includes the steps which have been followed for sample preparation. Figure 2.7 shows the prepared films of Pd on $1\times1cm^2$ glass substrate for XRD analysis. In case

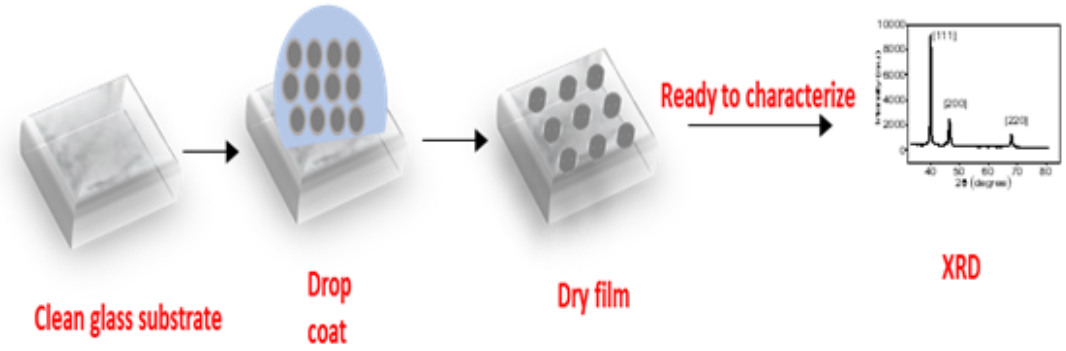

FIGURE 2.6: Schematic for XRD characterization.

of thin films, simple XRD techniques is not beneficial. X rays have high penetration depth on ultrathin films; so intense signals are obtained from substrate rather than from the ultrathin films. Thus, a special technique GAXRD is taken into account to attain the strong signals from the thin film surfaces. In this, incident angle is kept fixed at small values ($\sim$ 3-10^o), which decreases the penetration depth of X rays into the substrate; only the detector moves in the preset range. This helps to gather more information from the material of the film. More than one sample was studied for

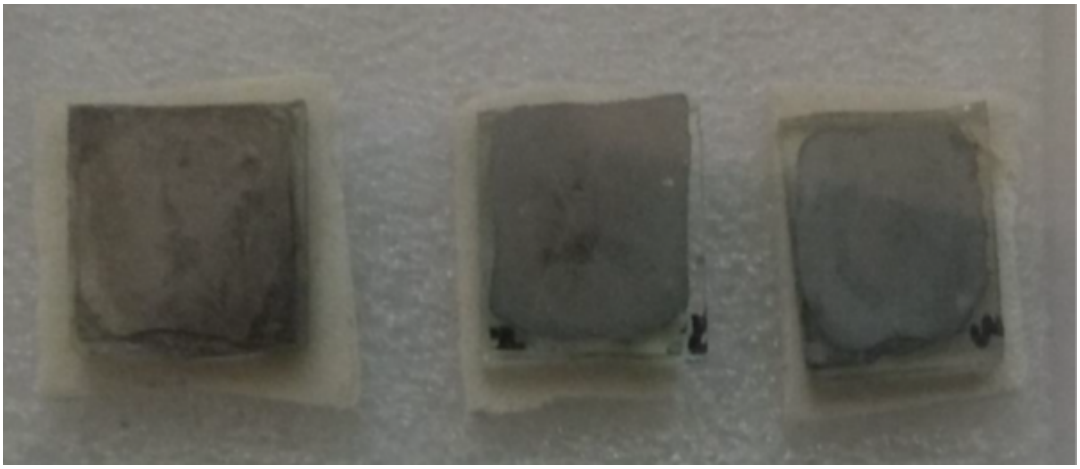

FIGURE 2.7: Prepared films of Pd on 1×1 cm^2 glass substrate for XRD analysis.

result confirmation.

2.5 DEVICE FABRICATION & SENSOR STUDY

On a 8x8 mm substrate (glass coverslip), thin film was developed by drop casting. The substrate is made rough by using a diamond pen. The nanoparticle dispersion ($\sim$ 0.05 ml) was put onto the substrate (2-drops) and dried. For electrical connections, silver paste and copper wires were used (Figure 2.8). Keithley picoammeter/voltage source (Model-6487) was used to record the electrical data during measurements.

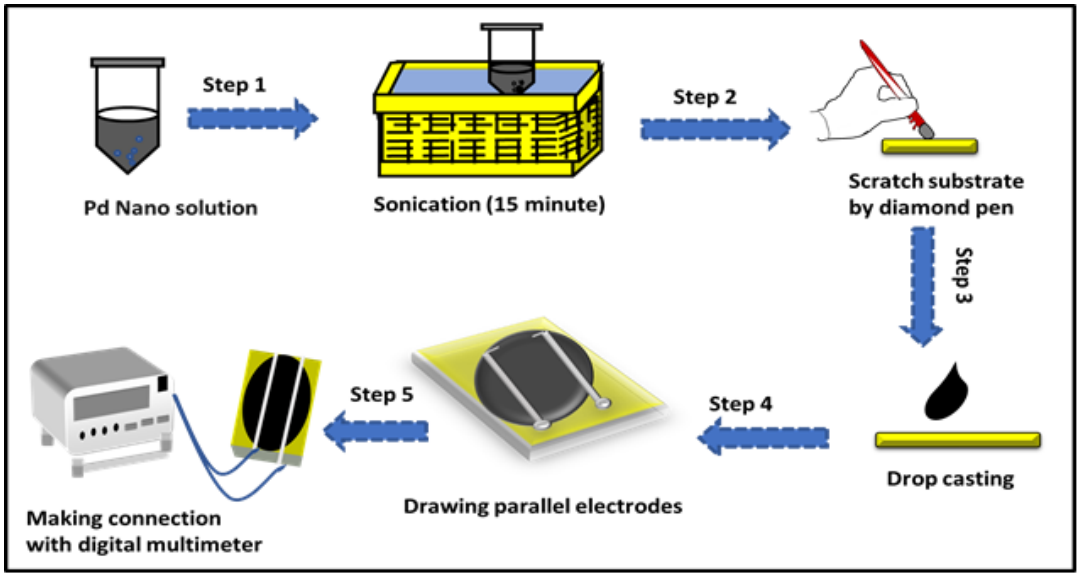

FIGURE 2.8: Schematic diagram for preparation and use of a resistive sensing device.

Nano film which has been coated to the substrate surface is merely a drop casting deposition of nano-dispersion. Although the substrate has been scratched before use so that film has a firm grip with the substrate, a transparent protective casing can also help to protect the film from the physical contact and to have prolong use of the device. In general, three kinds of electrodes connection were made by using silver painting. The most simplified form is parallel electrode connection which is named as single strand electrodes (Type 1, Figure 2.9). For a certain case if the film shows high resistance, then distance between electrodes can be reduced by simply giving U shape to parallel electrodes (type 2, Figure 2.9). Moreover, If the film is not uniform then interdigitated electrode connections are preferred. This is simply done by making perpendicular lines to the parallel electrodes at 1mm spacing to form a mesh like design so that all sections of the sensing film must be covered. Connections must be drawn carefully so that they do not join (type 3, Figure 2.9). Thin films of palladium

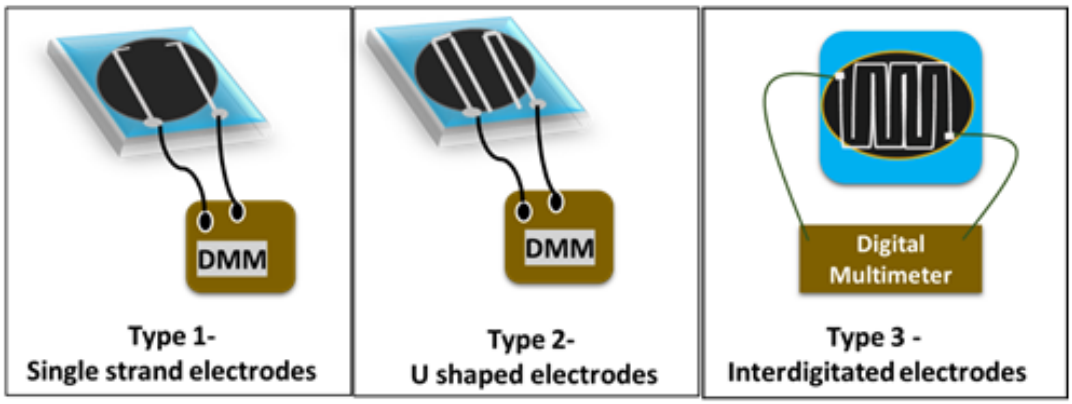

FIGURE 2.9: Classification of connection on the bases of designing of electrodes.

nanoparticles prepared by the above technique were used for the electrical studies. The very small resistance of these films was increased (to $\sim$ kohms) by incorporating 10 mg of glass powder in the nanoparticle-solvent solution prior to drop casting. Glass cover slips were crushed to prepare the glass powders [Figure 2.10]. The film resistance measurements were performed after laying the Ag-paste electrodes on the film and attaching fine copper wires. For the H_2 sensor studies, a small set up as

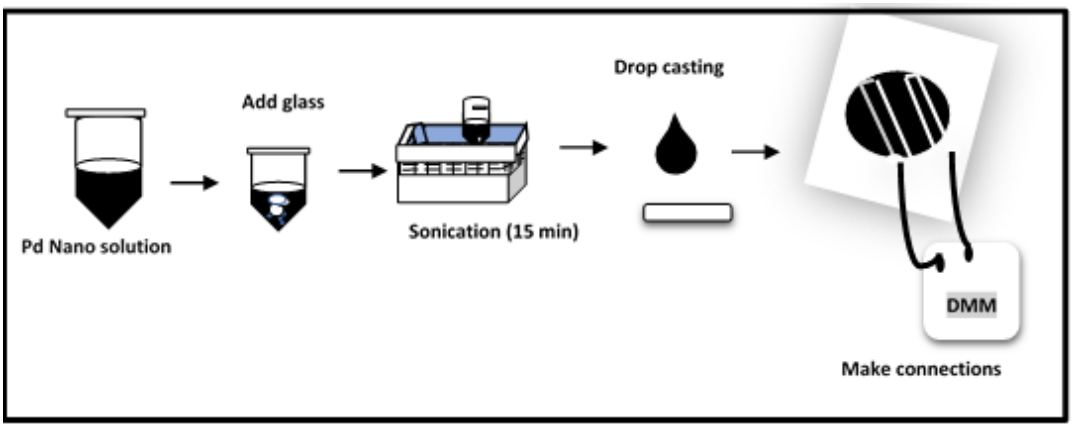

FIGURE 2.10: Glass mixed Palladium Nanofilms.

shown in Figure 2.11 was used. Flow controllers ["Make: Alicat Scientific, USA"] and a computer interfaced multimeter were used ["Model: Keithley 6487"] in the setup. The device is put in the glass furnace of the setup, whose temperature is controlled by PID controller (Figure 2.11). All measurements were performed under standard atmospheric pressure. Nitrogen was used as the carrier gas during experimentation. Firstly, the chamber was cleaned 2-3 times before use by simply flowing neutral carrier gas (e.g., N_2 gas/Air) to make the normal and moisture free environment of the

chamber. The test gas used for this study was hydrogen.

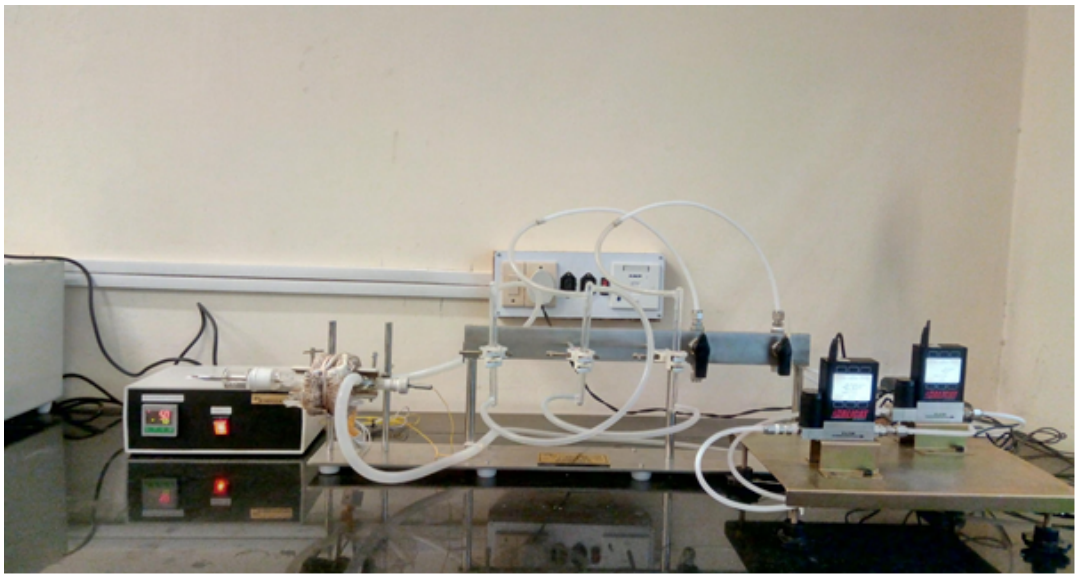

FIGURE 2.11: Gas sensor set-up.

Chapter 3

Effect of shape/size of palladium nanoparticles on the hydrogen response

In general nanomaterials have high catalytic efficiency compared to their bulk counterparts. In this regard, the potential of nanoparticles can be improved by changing certain characteristic synthesis control. For example, the size & shape of nanomaterials are particle characteristics that govern their catalytic property.

Both size & shape of the nano-yield are dependent on synthesis technique and synthesis parameters. The role of size and shape in catalysis has been analyzed from various angles by considering their synthesis technique [20, 47, 67, 72, 90]. For instance, the effectiveness of Pd NPs of different sizes was illustrated by considering the catalysis in "C–C coupling reactions" [76]. Basically, the surface to volume ratio of nanoparticles depends on their size. If this ratio is high, the catalytic activity of the nanoproduct is high. On the other hand, the shape of nanoparticles is due to the appearance of stable facets such as (111) or (100) on the particle surface. Each type of facet has different catalytic activity. It is reported that the (1 1 1) faceted nanocrystal are more efficient catalyst than (1 0 0) bounded nanoparticles for reducing Resazurin [11].

In this chapter, the hydrogen sensitivity of Pd nanocrystals is examined with respect to the variation of size and shape. Resistive hydrogen gas sensors were used for this study and the main emphasis was given for room temperature operation. The detailed experimentation is presented in Chapter 2 of this thesis. Four sample categories have been considered here for the discussion. They are palladium NPs synthesized with (i) 20% PVP, (ii) 32% PVP (iii) 45% PVP, and (iv) 60% PVP. The

size and shape characteristics of these samples were elaborately studied by using material analysis tools. Finally, the hydrogen sensitivity of these samples has been discussed with the help of suitable sensing schemes to understand the palladium-hydrogen interaction.

3.1 CHARACTERIZATION RESULTS AND DISCUSSION:

The work carried out in this chapter is based explicitly on the development of gas sensors using nanomaterials. Therefore, the surface morphology and distribution of the nanoparticles are the vital parameters to understand a sensing phenomenon. So HRTEM has been described in this chapter. The results of X-ray diffraction and UV-Vis Spectroscopy are also integral parts of this chapter. X-ray diffraction was used to determine the crystallite size and structural properties of the sample. The characterization techniques which were used for the research objectives are:

- GIXRD
- HRTEM
- UV-Visible Spectroscopy

3.1.1 GIXRD – crystallinity and size studies

The GIXRD is an approach for finding the crystallinity and size information. During the experiment, the atoms of the material cause a beam of incident x-rays to diffract in many specific directions. A simple relation for scattering angles is given by the Bragg's law (eqn 3.1):

$$2d \sin\theta = n.\lambda \tag{3.1}$$

Whenever Bragg's condition for constructive interference is satisfied, a reflection is produced. The average crystallite size of the nanoparticles is given by Scherrer's formula (eqn 3.2):

$$d = (0.9\lambda)/(\beta \cos\theta) \tag{3.2}$$

Here λ = 1.5406Åis the used X-ray radiation wavelength, β is the FWHM and 2θ is the diffraction angle.

For palladium, the planes (111), (200), and (220) corresponding to 2θ angles of 40.5^o, 46.7^o and 68.19^o respectively [JCPDS data (46-1043)]. Each material has a unique

XRD pattern. Therefore, by comparing the peak positions with the standard JCPDS data, it has been confirmed the presence of Pd element in the nano-yield. Sharp peaks in XRD data indicate the crystalline nature of the Pd. The three peaks of (111), (200), and (220) planes were deconvoluted so as to calculate the estimated crystallite size data (Figure 3.1) [5]. The asymmetrical peaks comprise of many peaks located at different 2θ values, and these peaks have different line broadening. Scherrer equation is used to calculate the crystallite size for each peak. These sizes are presented in Table 3.1. The deconvoluted peak intensity represents frequency/particle count; so the peak intensity vs corresponding particle size is plotted in Figure 3.2. It is apparent from Figure 3.2 that the particle size has a typical distribution that is changing with the change in stabilizer concentration. This distribution is further verified with the help of HRTEM results.

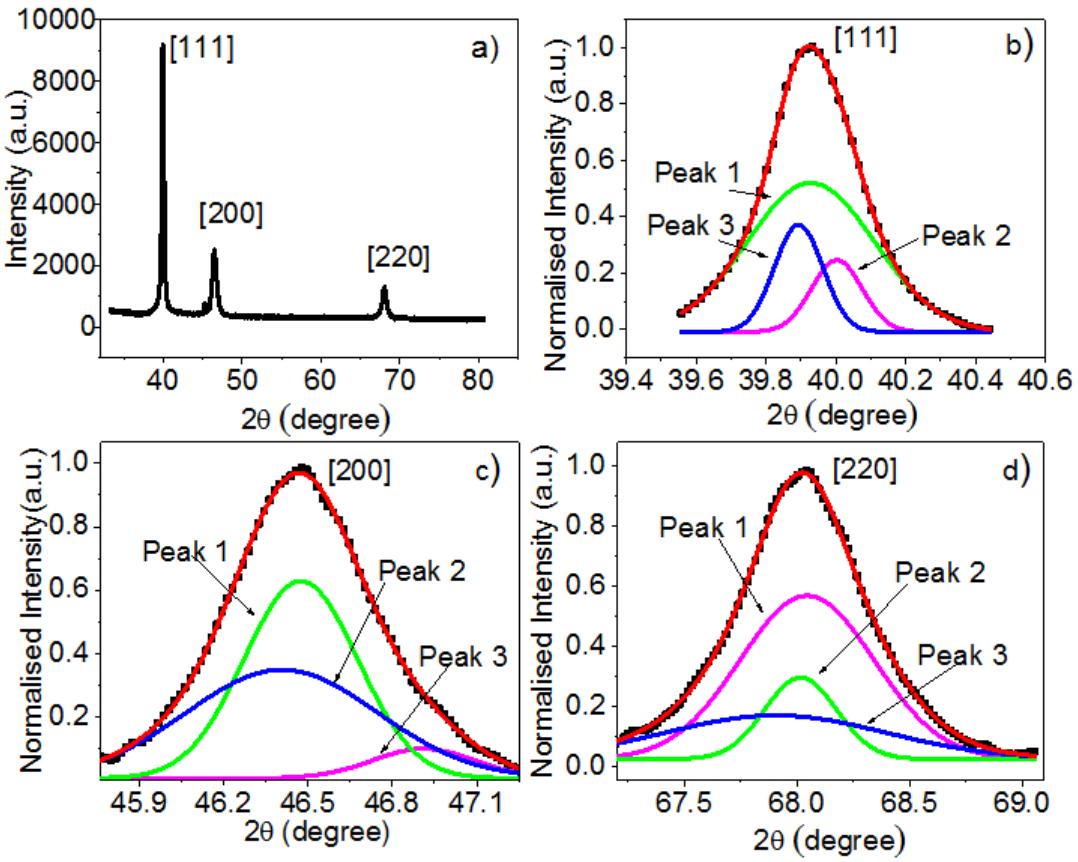

FIGURE 3.1: (a) GIXRD of Pd NPs synthesized with 32% PVP. (b) Deconvoluted (111) Grazing incidence X ray diffraction peak, (c) deconvoluted (200) Grazing incidence X ray diffraction peak, (d) deconvoluted (220) Grazing incidence X ray diffraction peak.

TABLE 3.1: Calculated size data from GAXRD data.

Sample	Planes	Size of crystallites
32% PVP	(111)	19.67 nm, 49.46 nm, and 51.66 nm
	(200)	10.79 nm, 18.2 nm, and 20.1 nm
	(220)	8.29 nm, 13.68 nm, and 25.43 nm
20% PVP	(111)	26.01 nm, 9.24 nm
	(200)	30.12 nm, 29.74 nm, 37.69 nm, 87.72 nm, 49.34 nm
	(220)	29.73 nm, 52.10 nm, 13.36 nm, 49.25 nm, 17.23 nm

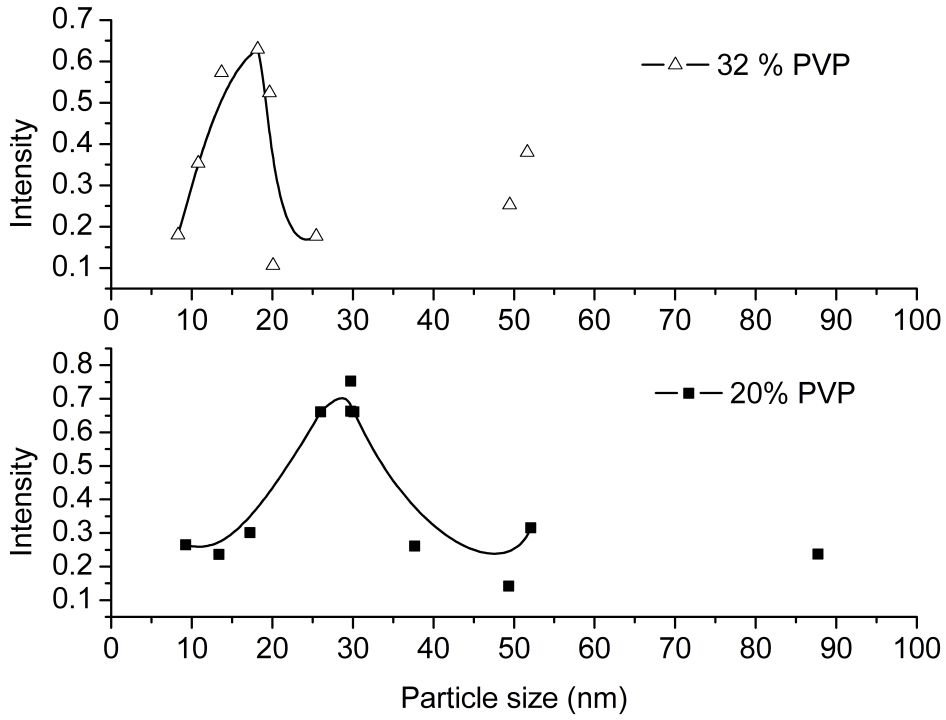

FIGURE 3.2: Nano size distribution of the samples (32% and 20% PVP) from x-ray diffraction data.

3.1.2 HRTEM – particle size and polydispersity studies

HRTEM is a technique in which an image is created from the interaction of the electron's transmission through the palladium nanoparticles. HRTEM images were analysed in two scales namely 20 nm and 200 nm which covers an appropriate range of particles distribution. It has been found that big sized particles (above 20 nm) are also formed with the small sized NPs (below 20 nm). The size uniformity of NPs is a big synthesis challenge for below 20 nm ranged particles. Therefore, the focus was put on the effect of polydispersity of NPs. It has been found that synthesis done with 32% PVP attains maximum polydispersity of palladium NPs; such a characteristic has been observed to be the reason of incredible sensing results (discussed

TABLE 3.2: Category I-small sized particles [20 nm scale]; Polydispersity in the synthesized samples.

PVP %	Mean diameter (nm)	Polydispersity index (PDI)
20%	13.37	0.0237
32%	12.59	0.0268
45%	11.79	0.0257
60%	10.75	0.0253

later). HRTEM images for the synthesized NPs are shown in Figure 3.3. The varia-

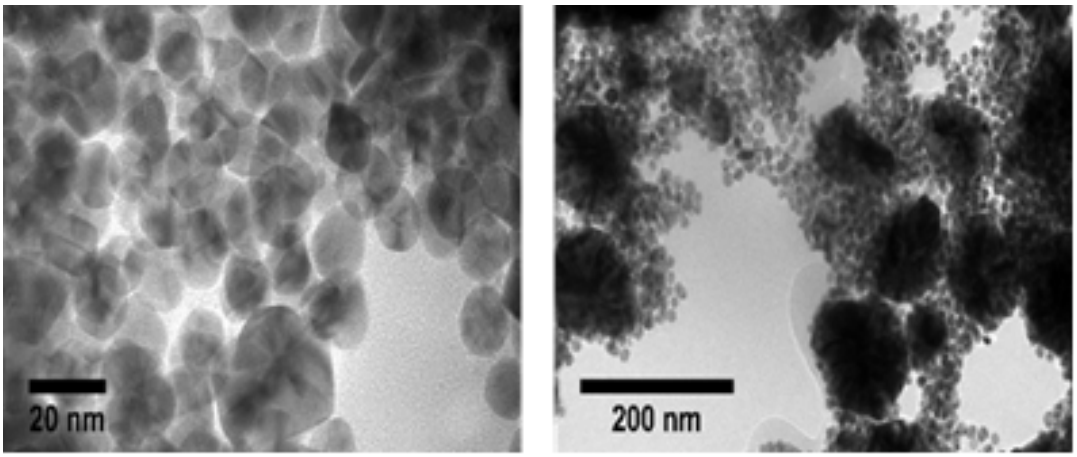

FIGURE 3.3: Pd-PVP 32% (mw 8000) NPs. a) small sized particles (20 nm scale) b) big particles (200 nm scale).

tion of particle size in the synthesized Pd NPs has been shown by histogram plots (Figure 3.4). The presence of two distribution curves indicate the broadening of size distribution which shows the existence of different size particles in large numbers. This also represent that the nanoparticle occurrences are more likely in two sizes which tells us about the frequency uniformity of same size particles present in 32% sample. However, one single size distribution curve is observed for 20%, 45%, and 60% samples. Thus,the particle count similarity of various sizes is observed from the bimodal fit of the 32% PVP sample for both small and large sizes (Fig. 3.4). Also, the smallest nano size ($\sim$10.45 nm) has been seen in this 32% category of PVP coted Pd NPs. This uniqueness of the 32% sample is further verified by the polydispersity calculation using HRTEM size data [Table 3.2 and Table 3.3]. It is evident that the polydispersity (i.e., size variation) is maximum for the 32% PVP sample (in both low and large size categories) (Table 3.2 and Table 3.3). The GIXRD results also indicated that the crystallite size is relatively lower in the 32% sample. Hence, from the above analysis (of broad distribution & highest polydispersity), it can be said that the 32%

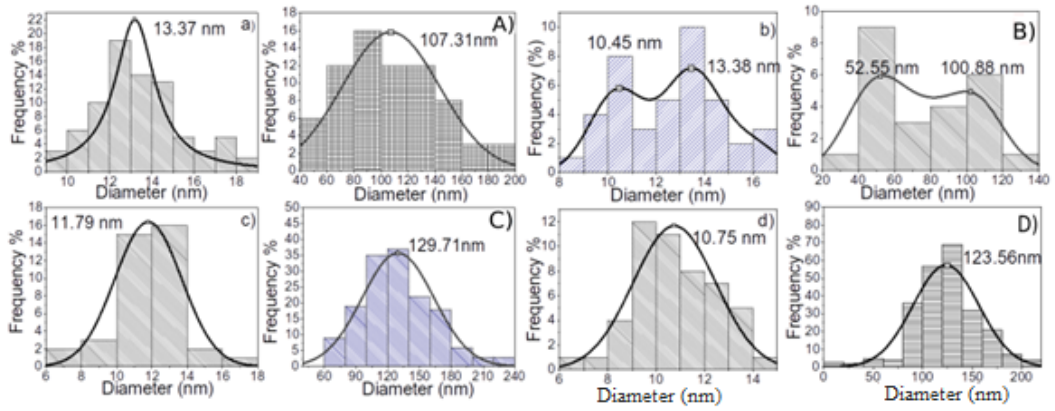

FIGURE 3.4: Particle size histograms for small range (a) 20% PVP, (b) 32% PVP, (c) 45% PVP, (d) 60% PVP for large range (A) 20% PVP, (B) 32% PVP, (C) 45% PVP, (D) 60% PVP.

TABLE 3.3: Category II- Large sized particles [200 nm scale]; Polydispersity in the synthesized samples.

PVP %	Mean diameter (nm)	Polydispersity index (PDI)
20%	107.31	0.1144
32%	74.73	0.1279
45%	129.71	0.0685
60%	123.56	0.0729

sample is really unique with respect to particle size and particle count uniformity.

HRTEM – Morphology (shape) and facet studies

The nano shapes are analysed with HRTEM images (Figure 3.5). PVP variation leads to the formation of shapes such as cuboctahedron (x = 0.20), octahedron (x = 0.32), decahedron (x = 0.45), and icosahedron (x = 0.60) (Figure 3.6). Large chunks of agglomerated nanoparticles were formed in the synthesis of Pd without PVP (x = 0.00) (Figure 3.5 b). SAED pattern shows the bright dot distribution in form of a com-

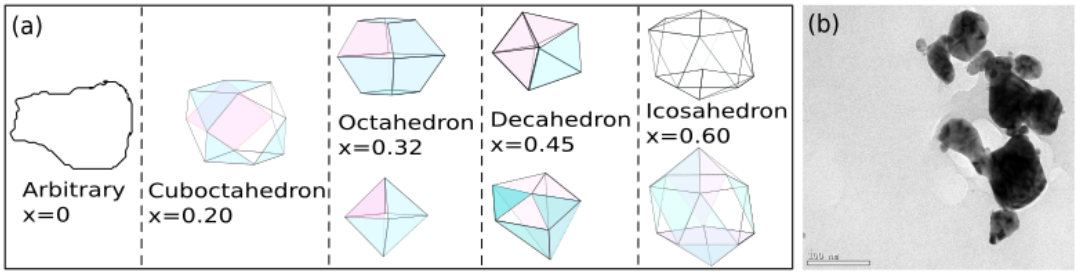

FIGURE 3.5: (a) Line drawing of ideal shapes for x = 0.00, 0.20, 0.32, 0.45, and 0.60 (b) Cluster of particles in x = 0.00 (scale = 100 nm).

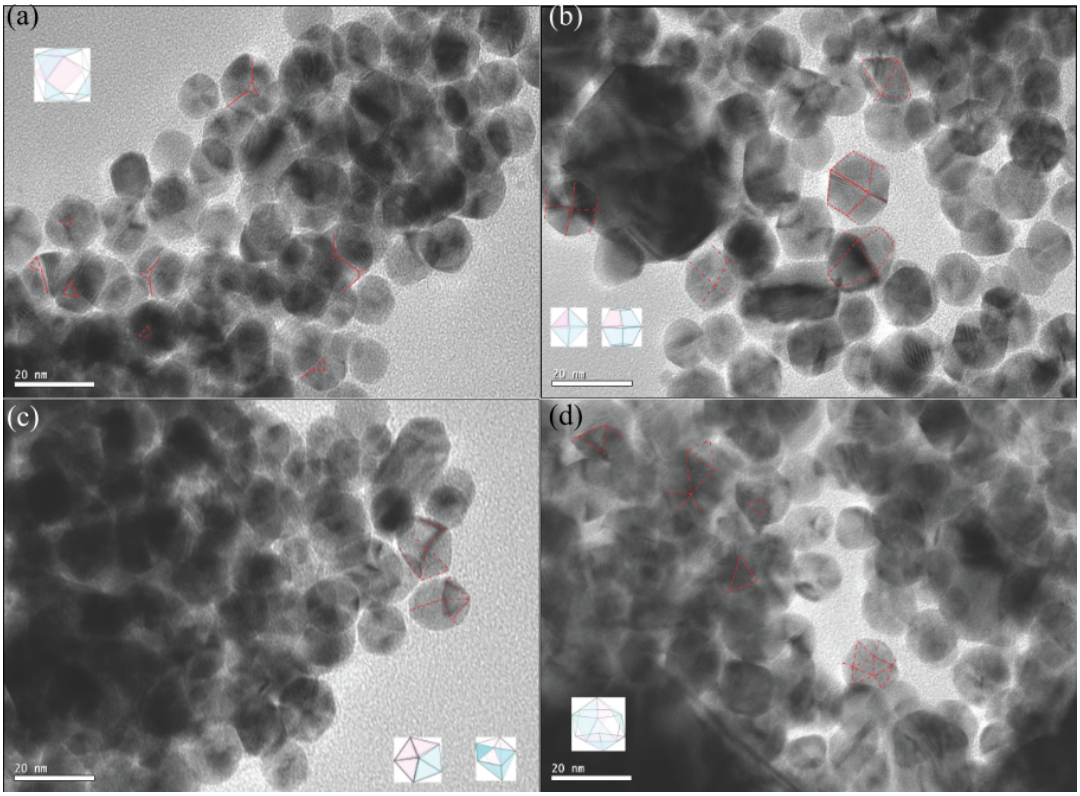

FIGURE 3.6: HRTEM images (scale = 20 nm) (a) x = 0.20 (b) x = 0.32 (c) x = 0.45 (d) x = 0.60.

plete ring which confirms the polycrystallinity of Pd NPs. The planar information is obtained from the SAED images (Figure 3.7 a-d) and the normalized electron diffraction intensities of the spotty rings is plotted in Figure 3.7 e. The high resolution images revealed a 0.22 nm (1 1 1) interplanar separation, which is compatible with FCC palladium. A characteristic rise in (1 1 1) peak intensity is seen with the rise in PVP amount. Also, the shapes are evolving with the increase in PVP concentration. This means new facets per particle is adding to the complexity. So, it is apparent that the (1 1 1) facets are gaining prominence with the rise in PVP concentration.

HRTEM-calculation of surface to volume ratio

The surface-to-volume ratio (S/V) tunes the catalytic response of Pd NPs. Table 3.4 represents the S/V ratio for shapes observed in this study. Hydrogen sensing is a surface catalysis phenomenon. So increase in S/V will imply increase in surface atoms. Such a activity trend towards the surface means comparatively better sensor performance. From Table 3.4 it is obvious that in the range x = 0.32-0.45, the S/V is high. In fact, these samples (x = 0.32-0.45) have excellent hydrogen sensing ability.

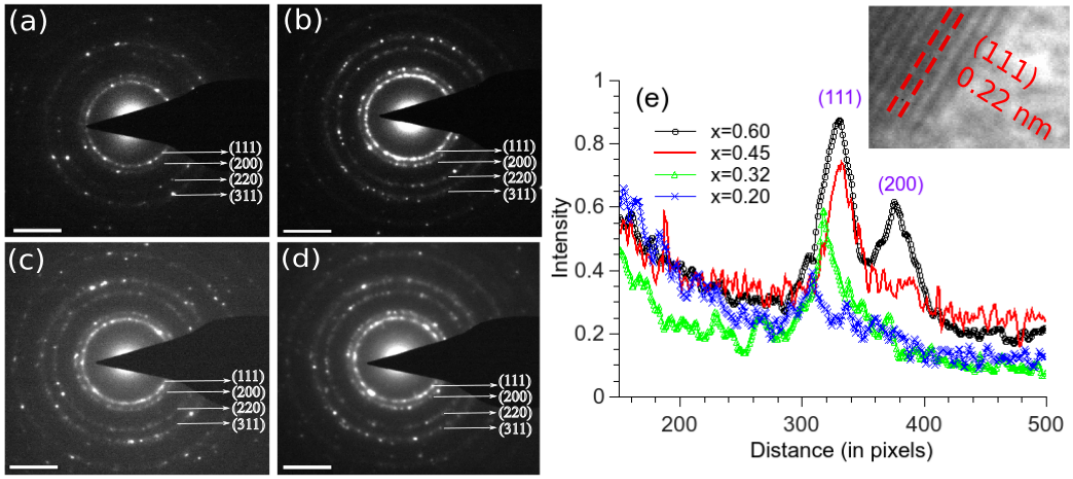

FIGURE 3.7: SAED patterns (Scale: 5 1/nm) of Pd NPs (a) x = 0.20 (b) x = 0.32 PVP (c) x = 0.45 (d) x = 0.60 (e) Intensity of (1 1 1) peaks.

TABLE 3.4: Calculation of S/V for various polyhedron shaped Pd NPs.

Shapes	**x**	**Edge length (a) nm**	**Surface to volume ratio (S/V) nm^{-1}**	**Formula used (S/V)**
Cuboctahedron	0.20	6.785	0.59	$(18+6\sqrt{3})/(5\sqrt{2}a)$
Octahedron	0.32	6.342	1.16	$(3\sqrt{6})/a$
Decahedron	0.45	6.300	1.14	$(5\sqrt{3}/2)/(((5+\sqrt{5})/12)a)$
Icosahedron	0.60	4.719	0.84	$(12\sqrt{3})/((3+\sqrt{5})a)$

Growth mechanism

Synthesis of nanoparticles involve nucleation and growth. The nucleation starts after the chemical reduction of precursor. In presence of stabilizer (such as PVP) the growth is moderated leading to uniform particle size. In this study, 0% PVP sample manifest non-uniform growth, and hence large clusters are formed due to uncontrolled agglomeration of generated nuclei. Even with PVP, the agglomeration partially eliminated because the quantity of PVP may not be sufficient to protect all particles properly. Hence large sizes exist alongside small sizes. Moreover speed of reduction reaction and the available synthesis time can also affect particle size. In this work, the synthesis time and temperature is same for all category of samples. The stabilizer PVP has a hydrophilic pyrrolidone head (HPH) and hydrophobic polyvinyl tail (HPT). The HPH passivate nano surfaces and HPT create stearic repulsion (SR) between nanoparticles. The HPH attaches by sharing a lone pair of

electrons (of the nitrogen atom) with the palladium surface. This is how the surface passivation is done. After the HPH attachment, the HPT generates a repulsive environment around the particle, which moderates the growth rate. So, the available amount of PVP in the reaction vessel is important to judge the uniformity in growth and this will imply that there exists some optimum concentration of stabilizer that will give good yield. So, if used stabilizer is less than this optimum value, uniformity will be reduced. For excess PVP (greater than the optimum value), the growth will be too slow due to the SR. However, if reduction rate is high, the initial agglomeration will be there because instanteous influence of HPH and HPT will not be available. This can be avoided by slowing the reaction and growth.

In this study, the optimum concentration is observed for the 32% sample and this optimum can be understood by taking into account the (PVP : metal) molar ratio. The significance of such a ratio was highlighted in the synthesis of PVP-coated ZnS nanoparticles [23]. Ghosh et al. reported a ratio magnitude of 0.007 as the optimum [23]. In this thesis work, the ratio for the 32% sample is 0.0139. So, probably anything close to 0.0139 will impart maximum surface protection of Pd NPs. Hence, the smallest nano-size (10.45 nm) is observed in the 32% sample. With the progress in synthesis time, the quantity of stabilizer (PVP) and precursor decrease. However, the (PVP : metal) magic ratio exists in the solution (for the 32% PVP sample). Therefore, multiple batches of particles with variable sizes are formed with the progress in reaction time. This is the cause of frequency uniformity (discussed with the help of HRTEM results) in the 32% PVP sample. For other samples (>32%PVP), size narrowing by SR effect is likely. Further in these samples (>32%PVP), the particle count is also reduced because of lower rate of growth for a period of 120 min (synthesis time). Similar study was done by Hei et al., where the (PVP: metal) ratio of $\sim$10 [35] The generation of shapes is related to the surface energy optimization of the various facets [such as (100) or (111)] in face centered cubic (FCC) palladium. For a FCC nanocrystal, PVP stabilizes the (100) planes easily [81]. The PVP branches stabilizes the (100) facets of palladium nanocube by lowering the surface energy. Now the various polyhedron shapes of nanoparticles evolve when PVP% is varied from 0% to 60% in the solution. This happens due to the generation of (111) facets at the cost of (100) facets in polyhedrons with increasing PVP quantity. Basically, the PVP stabilization of (100) facet is so high that it is in energy equilibrium with (111) facets. So, the (111) starts growing when PVP % is raised. This is also apparent from

the "selected area electron diffraction (SAED)" analysis of (111) plane for all PVP concentration. It has been observed that peak intensity of (111) increases with the increase in PVP amount. So, for low PVP concentration resulting shape is cuboctahedron that is dominated by (100) facets. With the increase in PVP, shapes like octahedron, decahedron, and icosahedron are obtained. These shapes are generated by the appearance of new (111) facets. However, the shape change can stop when the energy equilibrium is destroyed. Also, it is clear that the configuration of (111) facets increase from cuboctahedron to icosahedron. The cuboctahedron (having 6 + 8 = 14-surfaces) has the largest mixed morphology [i.e., both (1 0 0) and (1 1 1) facets]. Other shapes (octahedron, decahedron, and icosahedron) have only (1 1 1) facets.

3.1.3 UV-Vis

UV-Vis spectroscopy was performed to further verify the size variation. UV-Vis spectrum was deconvoluted into multiple surface plasmon resonance (SPR) peaks in the wavelength range 198-600 nm. The low wavelength (198-260 nm) absorption spectra are from small size NPs (Fig. 3.8 a-e). The spectrum (> 260 nm) are from large sized particles, and it comprises of low intensity peaks for all the samples. The low peak intensity probably indicates the existence of few particles. The spectrum after 260 nm is shown in Fig. 3.8 f (32% PVP sample). The UV-vis data reveal particle size and particle number abundance. The deconvolution technique for UV–Vis data analysis is reported in literature [8, 82]. The absorption wavelength increases with the increase in particle/cluster size. Data has been analysed in terms of peak broadening and wavelength shift as plotted in Figures 3.9 a, b. A red shift (until 32% PVP), and a subsequent blue shift, is observed for the 209 and 218 nm peaks (Figure 3.9). Such minor shifts occur because the samples have different particle sizes. Normally red (or blue) shift if observed can mean increase (or decrease) in size, respectively. Generally, the PVP abundance per unit area of particle surface is expected to rise with the increase in PVP. The low wavelength peaks (at 204 nm or less) are from small sizes. These small particles are easily protected by PVP. So, any rise in PVP concentration can reduce size because the rate of growth is moderated (lowered) due to increasing PVP capping, which seems to be saturated at 32% PVP concentration. Beyond 32% PVP concentration, due to a high concentration of capping agent, a micellar growth occurs which covers formed nuclei alongside nanoparticles. As a

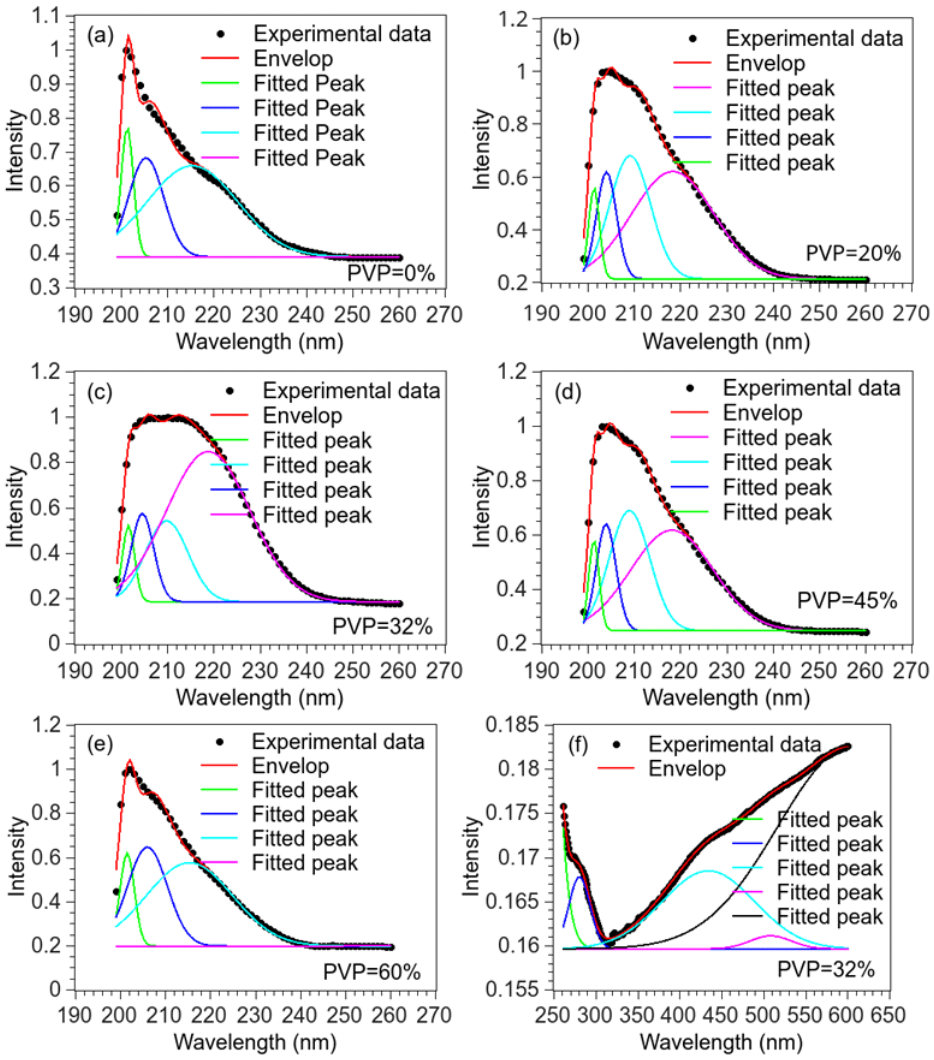

FIGURE 3.8: The UV–Vis fitted peaks for (a) 0% PVP, (b) 20% PVP, (c) 32% PVP (d) 45% PVP, and (e) 60% PVP; (f) 32% PVP sample (beyond 260 nm).

result, agglomerated clusters of small particles are formed. Therefore, the peak (near 204 nm) is redshifted after the initial blue shift (Fig. 3.9). The other peaks ($\sim$ 209 nm and 218 nm) are for bigger sizes. This big size happens due to the reduced PVP barrier around nanoparticles during growth. As we know that PVP helps in controlling growth of nanoparticles by shielding the outer surface. So, the tendency to form clusters increases if the shielding is poor due to the low PVP coverage. This is the reason for initial red shift for large sized particles (for $\sim$ 209 nm to 218 nm). The growth of these particles can also be retarded if large concentration of PVP branches are available, which is the case beyond 32% PVP. Hence, the peak has a blue-shift after the initial red shift for large cluster category of particles (209 nm & 218 nm) (Fig. 3.9). The UV–Vis absorption beyond 260 nm may be due to the agglomeration

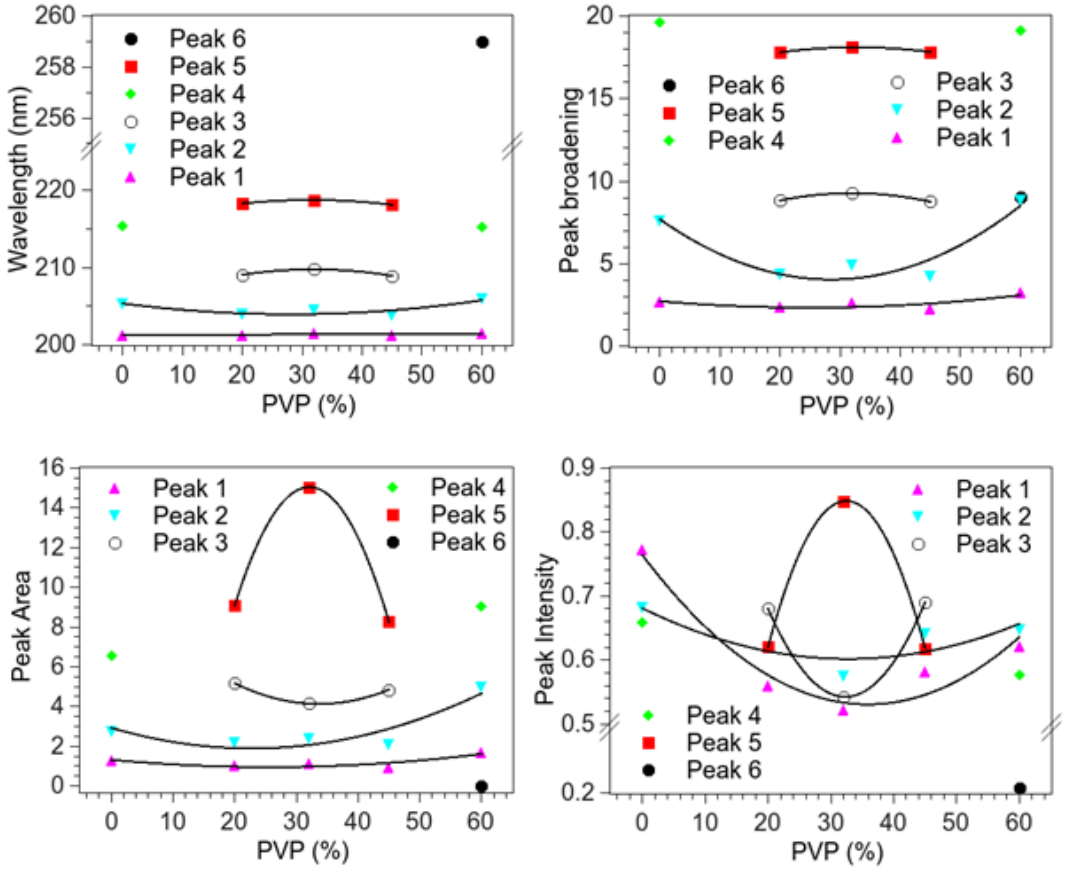

FIGURE 3.9: Plot of fitted UV-Vis peak parameters.

of small particles by micellar growth which shows the presence of very large sized particles/clusters [63]. Moreover, the presence of many UV-vis peaks at different wavelengths is an indication of polydispersity. Sometimes, the peak broadening is correlated to the dispersity in nanomaterials. Also, it is reported that broadening in SPR peaks may be caused by polydispersity of particles [37, 95]. In this study the peak broadening shows an optimum near 32% PVP sample highlighting the uniqueness of this sample (Fig. 3.9). The importance of this optimum correlates to the frequency uniformity in 32% PVP sample. The frequency of presence of similar sized particles is also obvious from the area (under the curve) and the peak intensity plot. Here also, an optimum is observed near 32% PVP concentration, which again refers to the speciality of this sample (Fig. 3.9).

TABLE 3.5: Baseline resistances for resistive devices fabricated with the samples

PVP %	Baseline device resistance at room temperature	
	Without glass powders	With glass powders
0	Negligible	Negligible
20		1.74 kΩ
32		0.91 kΩ
45		0.65 kΩ
60		1.78 kΩ

3.2 HYDROGEN GAS SENSING RESULTS AND DISCUSSION

Pure Pd NPs based films are conducting. The film resistance was increased by mixing powdered glass. In the films there are agglomerated clusters that provide the electronic shorted path. These shorted low resistance paths in the film were made discontinuous glass particles. The variation in baseline resistance for different samples has been tabulated in table 3.5.

3.2.1 Hydrogen gas sensing parameters

For data analysis the the change in device resistance (ΔR), which occur when the device is exposed to hydrogen gas is considered.
"% RESPONSE with respect to the original baseline resistance (R_o) = $((\Delta R/R_o) \times 100\%)$. RESPONSE TIME: The time taken by device to attain resistance value ($R_o \pm 0.9\Delta R$). RECOVERY TIME: The recovery time is defined as the time corresponding to the hydrogen OFF state when the device come back to its baseline value by 90%. The recovery time is the time taken by the device to attain resistance value of [($R_o \pm \Delta R$) - ($\pm 0.9\Delta R$) = ($R_o \pm 0.1\Delta R$] [5].

3.2.2 Working of palladium nanoparticle based resistive device in hydrogen ambient

When Pd atoms adsorb hydrogen gas atoms on its surface, there is abrupt change in electrical resistance of sensing film which is recorded by Keithley digital multimeter (DMM). A resistance versus time plot is done with the recorded data. This plot (also called whole sensing pattern) broadly comprises of two effects in terms of resistance

variation as shown in Figure 3.10: (i) Electronic effect: when hydrogen atoms adsorb

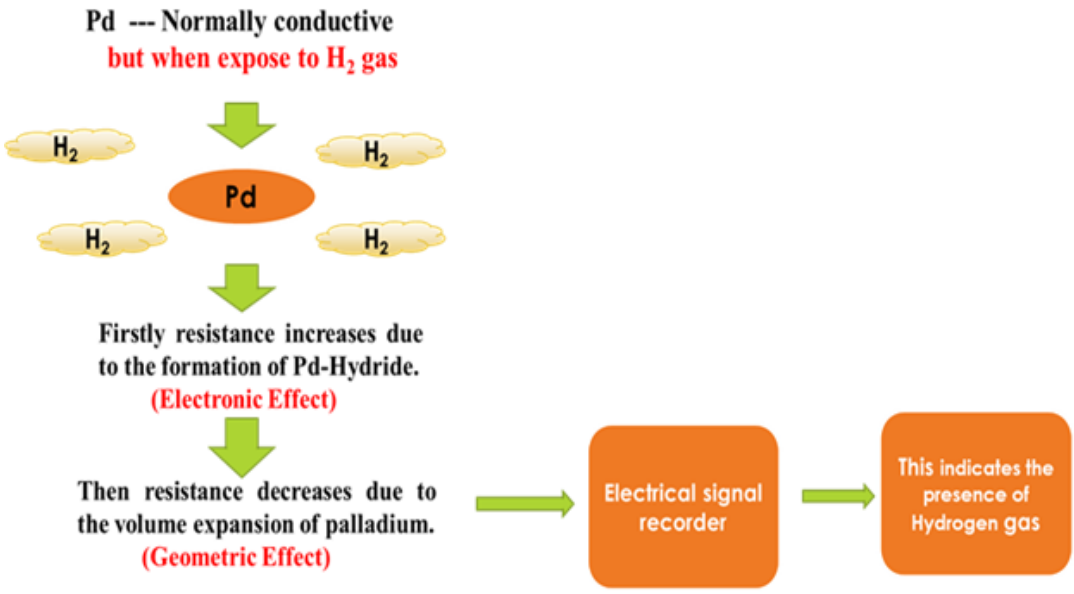

FIGURE 3.10: Palladium hydrogen sensing phenomenon-Electronic & Geometric Effects.

on Pd surface then there is increase in resistivity of palladium due to the formation of Pd-hydride (Pd-H_x). So, the resistance of the device increases.

(ii) Geometric effect: This effect comes after electronic effect. In this, device resistance decreases up to a large extent depending upon the adsorption of hydrogen gas atoms. This decrease in resistance happens due to the swelling of Pd atoms after adsorption, which reduces the interparticle barrier. Basically, the interparticle gap barrier is maintained by PVP coverage. This whole phenomenon is shown in Figure 3.10 and can also be realized in terms of the electron exchange (Figure 3.11). Initially the surface adsorbed oxygen is consumed and water molecules are formed. This process cleans the palladium surface and the active adsorption sites are now available for further hydrogen adsorption. The second step is the simple adsorption of hydrogen in palladium without any electron exchange. This produces palladium hydride, which has relatively larger resistivity than Pd. So, the film resistance increases, which is termed as the electronic response. Subsequently, the adsorbed hydrogen atoms now start the electron exchange with the palladium in the third step. This generates excess electron in the sensing film, which reduces the film resistance decreases drastically. Such a sharp change in resistance is termed as the geometric effect. Thereafter, the recovery process starts and the adsorbed hydrogen slowly gathers electron and becomes hydrogen atoms; and two hydrogen atoms join

to form the hydrogen molecule. This hydrogen molecules escapes. Such a reverse process slowly increases the device resistance towards the baseline value. Finally, with the help of atmospheric oxygen impurities, the protective oxygen coverage is again established.

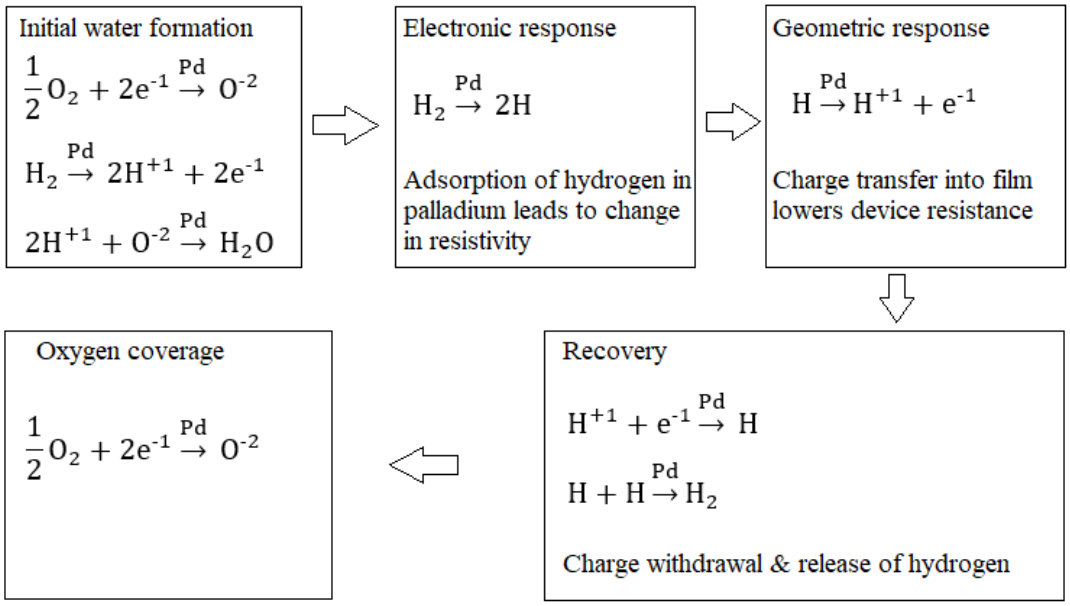

FIGURE 3.11: Electron exchange during palladium hydrogen interaction-Electronic & Geometric Effects.

3.2.3 Sensing data and analysis

In this study, the films prepared with 0% PVP sample showed no response for H_2. Other samples (PVP 20%-60%) are sensitive to hydrogen (Figure 3.12(a)). This difference is governed by the interparticle surface barrier that is not available in 0% PVP sample as it comprises of only large chunks. Basically the PVP branches on the nanoparticle surface creates sufficient interparticle separation for the execution of the geometric effect. The overall device response is presented in (Figure 3.12(c)) at different hydrogen concentrations. The resistance change (ΔR) varies with the change in hydrogen concentration. The overall sensing mechanism (discussed earlier) comprises of generation of water molecules followed by electronic/geometric effects. These are responsible for the cause of the resistance change shown in Figure 3.12.

The 0% Pd-PVP sample comprises of only large chunks and these chunks remain in contact even after addition of glass particles. So no geometric response is possible

for the 0% Pd-PVP sample. Any minor change in device resistance of the 0% PVP sample may be attributed to the electronic effect (occurring in the chunks). However, these minor resistance changes can merge with the noisy baseline and may not be clearly observed. Hence, the 0% PVP is insensitive to hydrogen.

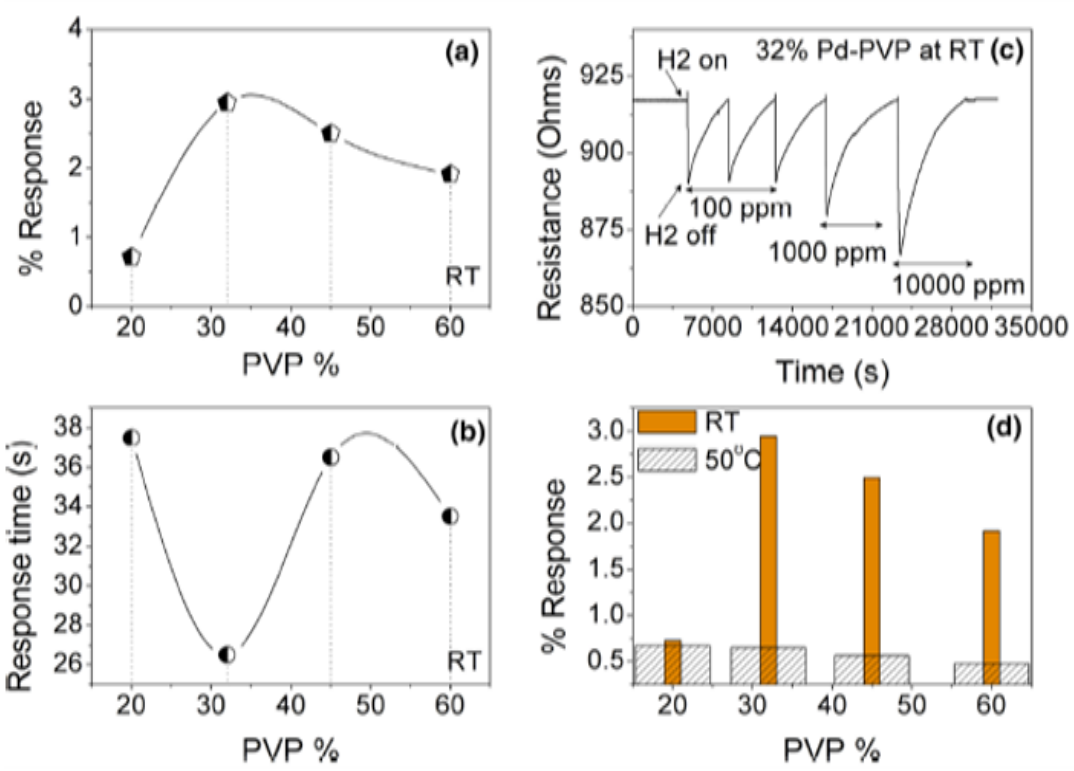

FIGURE 3.12: H_2 response parameters: (a) % response vs PVP concentration (100 ppm H_2), (b) response time vs PVP concentration (100 ppm H_2), (c) repeated cycles by varying H_2 concentration, (d) % response vs operating temperature.

Role of glass powder in the sensing film

The shorted electronic path in the sensing film is to be isolated because they impart negligible resistance to the device and nil hydrogen response in all categories of samples. Glass particle helps to introduce discontinuity in those shorted paths. Of course this is not a selective phenomenon because glass particle can also bring discontinuity in good uniform barrier path. Nevetheless the shorted paths are definitely eliminated because the overall device resistance changes from negligible to appreciable value after addition of glass particles. The shorted paths are due to presence of large clusters in the films. This phenomenon of activation of uniform barrier (created solely by PVP) paths is presented in Figure 3.13(a) (b).

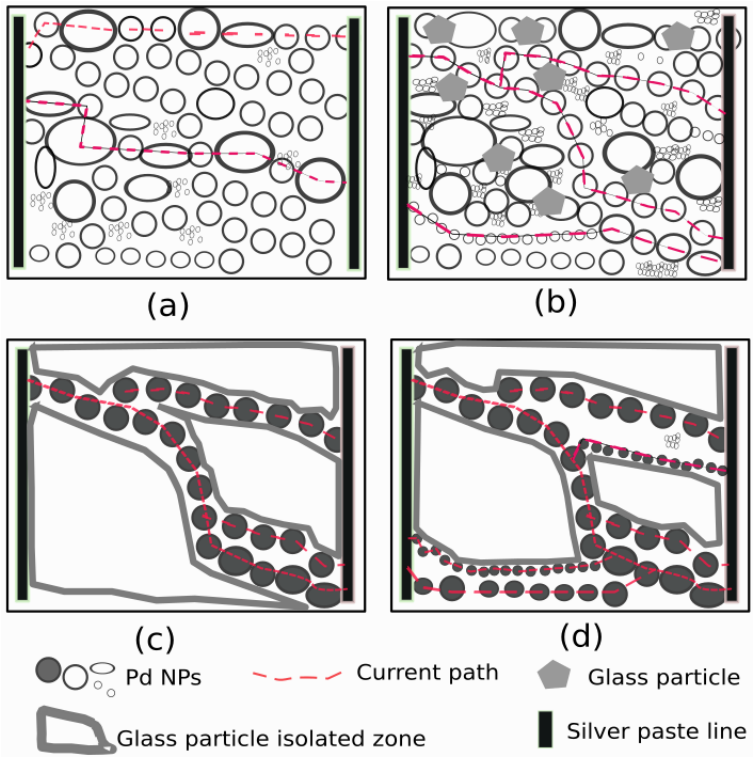

FIGURE 3.13: (a) Electrically shorted electronic path (without glass particles) (b) discontinuity in shorted current paths and activation of electronic paths having uniform barrier (with glass particles) (c) many paths comprising similar-sized particles ("monodisperse") (d) many paths comprising variable sized particles ("polydisperse").

Role of PVP in the sensing film

The interparticle gap is created by the PVP branches residing on the particle surface.The distribution of the branches is different for the samples synthesized with different PVP concentrations. Nanoparticles with high surface activity acquire good PVP coverage in order to passivate the surface. Other particles having poor PVP coverage agglomerate to form large chunks during growth. These chunks are not useful for hydrogen sensing. Nanoparticles (with uniform PVP coverage) in the sensing films have the required interparticle barrier to undergo both electronic and geometric sensing effects sequentially. For non-uniform surface coverage, the interparticle barrier will be negligible and will be a hindrance to good hydrogen sensing. Normally these uniform PVP covered nanoparticles form small useful current paths (as presented in Figure 3.13), and the hydrogen absorption in these uniform barrier paths will be influenced by particle size and particle count. This is discussed in the next section.

Role of size dispersity in sensing

For a spherical particle, the surface/volume ratio varies as (1/r) where 'r' is the size (radius). Also, the paths highlighted in the sensing mechanism will increase in length if the particle count is high and vice versa. This variation in path length (or particle numbers) will vary the hydrogen absorption. This study reveals that the 32% PVP has the smallest particle size and particle count uniformity (between different sizes) in a polydisperse matrix, which is apparent from the HRTEM studies. All these particles in the 32% PVP sample will acquire good PVP coverage and will form multiple electronic paths with uniform barrier (Figure 3.13). However, for other samples such polydispersity variation is relatively low and so the number of paths with uniform barrier will be comparatively less. Hence, this variation in size and polydispersity will definitely enhance the hydrogen adsorption magnitude in the current paths (shown in Figure 3.13) for the 32% PVP sample. For the 20%, 45%, and 60% PVP based samples having low polydispersity and relatively bigger particle size, the hydrogen absorption is expected to be lower than the 32% sample. Therefore, from this viewpoint, 32% PVP is the best sample for hydrogen sensing at RT. The time of response for device saturation is dependent on the geometric effect, which is comparatively faster. The geometric effect in turn depends on the interparticle PVP barrier, which may not be uniform in all the current paths for all the samples. Such a barrier variation can lead to variation in the intensity of the geometric effect in individual current paths (as shown in Figure 3.13) for different samples. Since the time of response is minimum for the 32% PVP sample (Fig. 3.12b), the geometric effect saturate easily, & for other samples it will take relatively more time to finish. The quick saturation of the geometric effect is controlled by the particle morphology, which is discussed in the next section. Interestingly, the magnitude of this response time is not very low all the samples. Even for 32% PVP sample it is still very large. This can be attributed to the association of the bulk of the films via hydrogen diffusion. Hence the desirable condition is to restrict the hydrogen activity within few nanoparticle layers in the vicinity of the top surface of the film. If the whole phenomenon confines to one layer of Pd NPs, the response time would be lowerd. However, in drop casting technique, monolayer formation is experimentally difficult.

The time of device recovery time high ($\sim$ minutes). This implies a slower desorption rate, which may be due to hydrogen trapping inside palladium. Alternately the

involvement of the bulk of the palladium films can delay the recovery of the device. Hence, in this chapter, the recovery times are not compared. Further studies may give important breakthrough to improve the recovery characteristics. The repeated patterns reveal reproducible behaviour of the devices at RT (Figure 3.12c).

Role of morphology-dominance of (111) facets in hydrogen adsorption

The H_2 response behaviour and the particle surface morphology can be correlated. From the HRTEM studies the increase in (111) facet bounded morphology with the increase in PVP concentration is apparent. Also, the stability with respect to energy of (111) facet is higher than (110) or (100) facets in face centred cubic palladium [9]. HRTEM studies also reveal that the cuboctahedron has mixed faceted morphology (i.e., both (100) and (111) facets) with (6 + 8) = 14 surfaces. Other shapes (octahedron, decahedron, and icosahedron) have mainly (111) facets, and the count of surfaces for ideal shapes are 8, 10, and 20 respectively. Normally, the hydrogen activity of (111) facets are higher than (100) facets for palladium particles [11]. It is also well known that the hydrogen adsorption ability of (100) and (111) facets are similar in palladium. However, the palladium-hydrogen interaction on (111) surface is relatively faster than (100) surface [54]. Also, the hydrogen desorption from (110) facet is comparatively higher [50]. Therefore, for fast catalysis with H_2, Pd (111) facets are important. It can be speculated that during palladium nanoparticle-Hydrogen interaction the magnitude and speed of response are entirely dependent on the total (111) facet area. The best hydrogen activity is obtained in samples synthesized with 32% PVP (Figure 3.12), where the time of response minimizes and the %response maximizes. Hence it is obvious that the nanoparticles have near ideal shapes and the total (111) facet area is maximizing in the vicinity of 32% PVP concentration.

Theoretical evidence for 32% PVP

This change in sensor performance with change in temperature is analysed by evaluating Arrhenius activation energies [29]. Equations (Eq. 3.3) are useful to calculate $\Delta E = E_A - E_H$, which is the change in activation energy while shifting from air to hydrogen. In this case E_A and E_H are the energies of activation in air and hydrogen

respectively.

$$\begin{aligned} \ln(R_A) &= \ln(R_o) - E_A/kT \\ \ln(R_H) &= \ln(R_o) - E_H/kT \\ \frac{R_A - R_H}{R_A} &= 1 - \exp\frac{\Delta E}{kT} \end{aligned} \tag{3.3}$$

The device resistances in air (R_A) and in H_2 (R_H) are necessary to evaluate ΔE. Figure 3.14 is plotted between ΔE and 'x'. Here 'x' is the ratio of PVP & precursor. Figure 3.14 reveals that at all temperatures the difference in activation energy (ΔE) is negative for all samples. This means $E_A < E_H$. Such an inequality indicates that in hydrogen atmosphere all low energy active sites are occupied and the remaining high energy sites are available for hydrogen adsorption. Another conclusion can be drawn from the magnitudes of ΔE at RT and 50°C. Compared to RT, ΔE is low at 50°C for samples in the x range 0.32 - 0.60, while it is high for x = 0.20 sample. This means the high temperature sensitivity of x = 0.20 sample is comparatively better. Moreover, the optima of ΔE at RT and 50°C are also obvious (Figure 3.14). The RT optimum indicates that for best performance the range of x must be 0.32 < x < 0.45. Also, from the optimum at 50°C it can be stated that x ≤ 0.20 is suitable for high temperature applications [4].

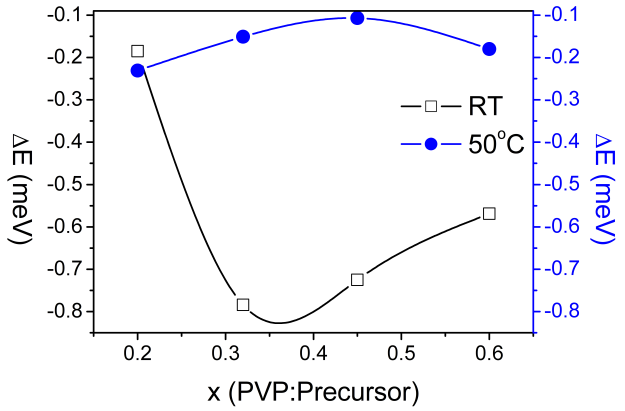

FIGURE 3.14: Arrhenius activation energies.

3.3 SENSING STUDY AT HIGHER TEMPERATURE

At high temperatures the sensor performance deteriorates (Figure 3.12d). This deterioration in % response at elevated sensing temperature (50^oC) is probably due to the enhanced hydrogen desorption relative to absorption. It can be speculated that any further rise in temperature will not improve the response. Therefore it is apparent that these films are suitable for RT hydrogen sensor applications. The high temperature performance of the 20% PVP sample is relatively better than the other samples. This is attributed to the mixed facet characteristics of the 20% PVP sample. The cuboctahedron shapes in this samples have both (100) and (111) facets. So, the (100) facets might have relatively better hydrogen adsorption ability at high temperature. Rest of the samples are dominated by (111) facets. So, their room temperature performance is superior.

3.4 EFFECT OF HUMIDITY ON SENSING PERFORMANCE

The influence of moisture on the device characteristics must be analyzed because water molecules could be retained by the PVP chains on the particle surface. 65% and 75% humidity concentrations were selected for this study. The 32% sample was used. The sensor results varied when the relative humidity was increased (Table 3.6). As presented in Table 3.6 that at RT, the rise in moisture content deteriorates the %response and improves the response time. However, at 50^oC, both these parameters improved. The discussed mechanism considered the generation of water molecules when the sample is exposed to hydrogen. Hence an additional rise in humidity will lead to more retention of moisture at the PVP covered nanoparticle surface. This may block active surface absorption sites and reduced number of available active absorption sites for hydrogen adsorption. Thus the % response deteriorates at room temperature, as the material surface now adsorbs less hydrogen. So, a quick saturation of solid-gas interaction is likely. Since the sensing phenomenon involves electronic (slow) and geometric (fast) effects, the quick saturation can also indicate accelerated geometric activity. This is probably the reason for the betterment in the time of response at RT when humid concentration increased. At 50^oC, due to higher available thermal energy, the moisture release from the PVP covered particle surface is comparatively better due to improvement in evaporation rate; this is the reason

TABLE 3.6: Influence of moisture on the sensor parameters (in 100 ppm H_2) for the 32% PVP sample

	At room temperature		**At 50^{o}C**	
Humidity %	**% response**	**Response time (s)**	**% response**	**Response time (s)**
65	3.07	48.5	0.53	31
75	2.95	26.5	0.64	30.5

for the slight change in the response parameters. Due to technical difficulties, other values of relative humidity could not be selected for this study.

3.5 CONCLUSION

Finally with respect to the starting objectives, it can be summarized that size/shape attributes of Pd NPs play a crucial role in determining their interaction with hydrogen. Especially, in hydrogen sensing, the size and shape critically affect the response parameters. The operating temperature of palladium nanoparticle-based hydrogen sensors can be easily justified if these size and shape corelation is established. The PVP concentration is a potential factor for the size and shape modulation (facet generation) in polyol synthesis of Pd nanoparticles. It is observed that 32% PVP coated NPs have octahedron shapes with high S/V ratio and maximum polydispersity.

Chapter 4

Role of stabilizer (Mw 8000) coverage on nanoparticle surface on the hydrogen-palladium nanoparticle activity

The surface activity of nanoparticles is an important concern for catalytic application especially gas sensors. Same material having differences in surface activity can manifest difference in catalytic activity. The surface activity can be tuned by incorporating synthesis variation [1, 6, 13, 48, 66, 75]. PVP chains act as stabilizer and are used in the surface passivation of nanoparticle surfaces. Variation in surface coverage can be monitored by optical characterization tools such as UV-Vis spectroscopy, *etc* [62, 83, 97]. PEG ("Polyethylene glycol") variation on "polystyrene" nanoparticles was found to impart stability in drug delivery [7].

The hydrogen sensitivity of palladium (Pd) nanoparticles based devices can be tuned if the nanoparticles are washed with different solvents before device fabrication. In this chapter, the role of washing the Pd nanoparticles with either distilled water or ethanol on their hydrogen sensitivity is presented. The change imparted in the surface properties of Pd NPs after washing is reviewed with UV-Vis spectroscopy and GIXRD studies. From the GIXRD data, the nature of strain is particularly analysed to evaluate the sensing mechanism. The synthesis methodology for this study is discussed in detail in Chapter-2.

4.1 CHARACTERIZATION RESULTS AND DISCUSSION

The characterization techniques which were used to fulfil this research objective is:

- GIXRD
- UV-Visible Spectroscopy

4.2 GIXRD

The face centred cubic crystallinity of the samples (washed in water and ethanol) is apparent from the three intense peaks (Figure 4.1). The (111) peaks are separately compared, and is 0.16-degree shift is observed (Figure 4.1). The other two peak (200) and (220) shifts are tabulated in Table 4.1. Maybe the oxygen contamination during film preparation is the cause of this fine shift. Only films of these materials are likely to gather oxygen impurities. The amount of oxygen contamination is likely to be different in the two sample categories due to variation in PVP surface coverage. Since similar films are also used for sensing, the reference to surface oxygen contamination is also discussed in the context of hydrogen gas sensing. This oxygen contamination on the nanoparticle surface is also the reason for the difference in the calculated strain from GIXRD data.

To evaluate the strain, the 2θ data of the peaks and the "peak broadening" (β) values are used to calculate $\beta \cos\theta$. Williamson-Hall (W-H) plot ($\beta \cos\theta$ vs $\sin\theta$) for each sample category reveal both the nature and magnitude of strain (Figure 4.2). The strain is estimated from the slope of the linear fit (Figure 4.2) [71]. Both samples have tensile strain (due to positive slope of fitted line). However, strain magnitude is relatively greater in samples washed with water. The values of strain are 0.01536 and 0.01053 for samples washed with water and ethanol respectively. For hydrogen sensing using palladium nanoparticles, high strain can increase the catalytic effect [22, 80]. So, comparatively large strain in samples washed with water is likely to make the hydrogen sensing better than ethanol washed category.

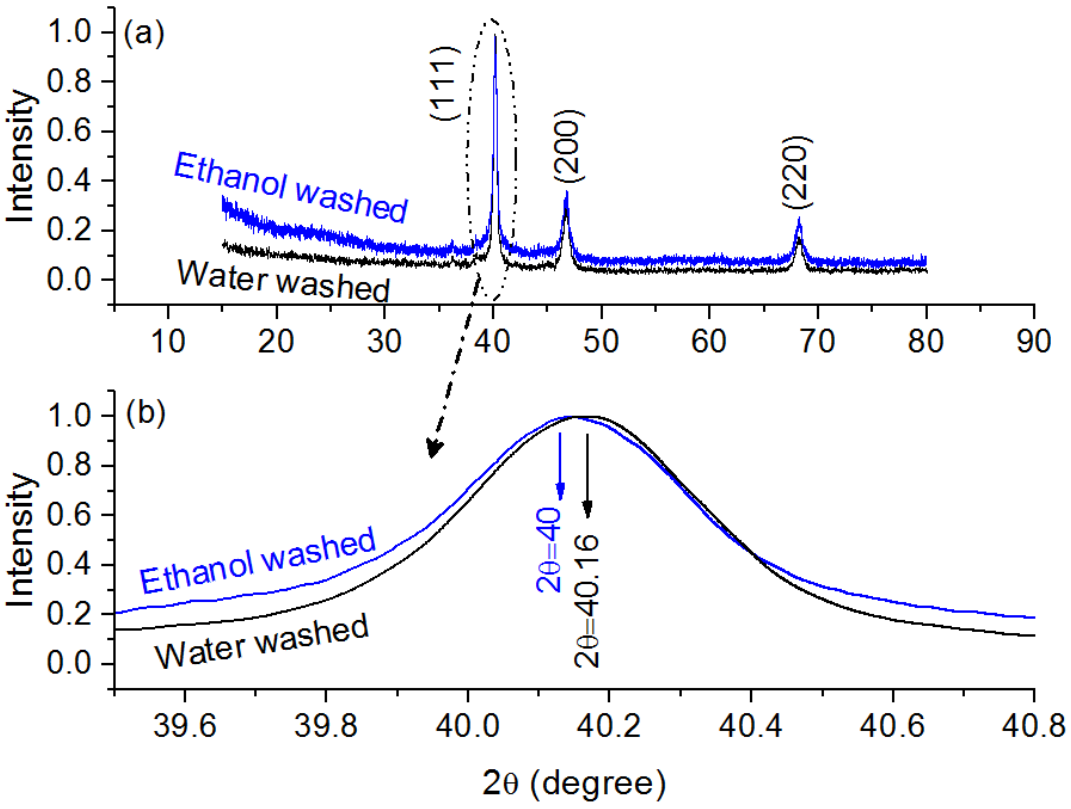

FIGURE 4.1: GIXRD spectra of the two category of samples (a) Full spectrum (b) (111) peak shift.

TABLE 4.1: Peak positions

Peaks	2θ value	
	Water washed	**Ethanol washed**
(111)	40.16	40
(200)	46.74	46.72
(220)	68.22	68.18

4.3 UV-Vis

UV-Vis data (shown in Figure 4.3) compares ethanol and water washed samples. Basically, their absorption wavelengths are used for comparison. Using peak deconvolution technique, the characteristics peaks for each spectrum are obtained (Figure 4.3) [8, 82]. The absorption wavelengths from the fitted peaks lie in the UV range. Slight change in size of nanoparticle, or the PVP surface coverage can shift the UV-Vis pattern. Since, the main difference between the two sample categories is the surface PVP coverage, the variation in the UV-vis results may also be attributed due to the differences in PVP [97]. It is reported that ethanol can attack the PVP layer on the nanoparticle surface [25]. So, most of the PVP chains are discarded while the

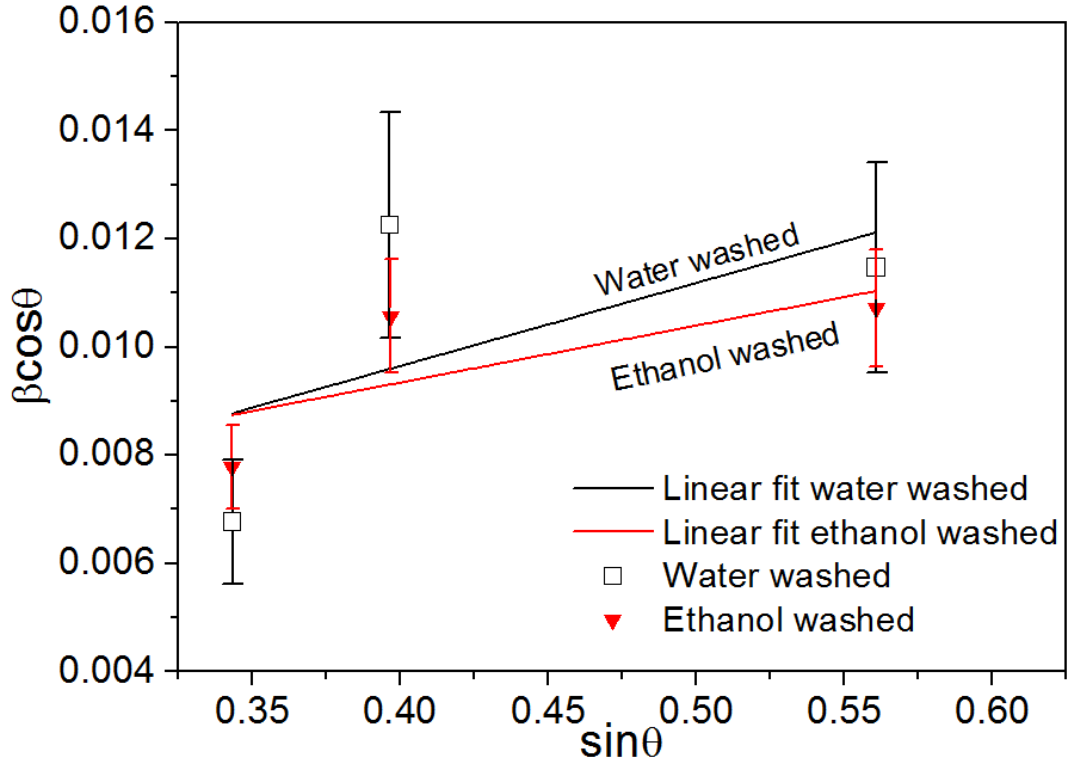

FIGURE 4.2: W-H plot for samples washed with water and ethanol.

sample is washed with ethanol. On the other hand, water has no effect on the attachment of PVP and nanoparticles.

From the deconvolution of water washed spectrum 8-peaks of variable intensities are obtained for the total wavelength range 190-600 nm. The lowest peak wavelength is ∼190 nm, and it may be assigned to the smallest nanoparticle size. The rest of the peaks can reveal the existence of other particle sizes in ascending order (from small to large). Since the spectra is for water washed sample, all particles have a dense PVP protection on the surface. For samples washed with ethanol, the PVP layer on particle surface is not sufficient to fully passivated the nanoparticle surface. Hence very small sized nanoparticles cluster together and relatively large sized nanoparticles are generated. These big sized NPs can red-shift the absorption peak. The deconvoluted ethanol washed spectra reveal minimum absorption wavelength of 201 nm, which is 11 nm red-shifted with respect to the smallest absorption wavelength for samples washed with water. Moreover, in the range 190-260 nm, four peaks in water washed sample and eight peaks in ethanol washed sample are observed. So, the cluster size variation due to scare PVP coverage in ethanol washed samples is quite apparent from the no of peaks. Both water washed and

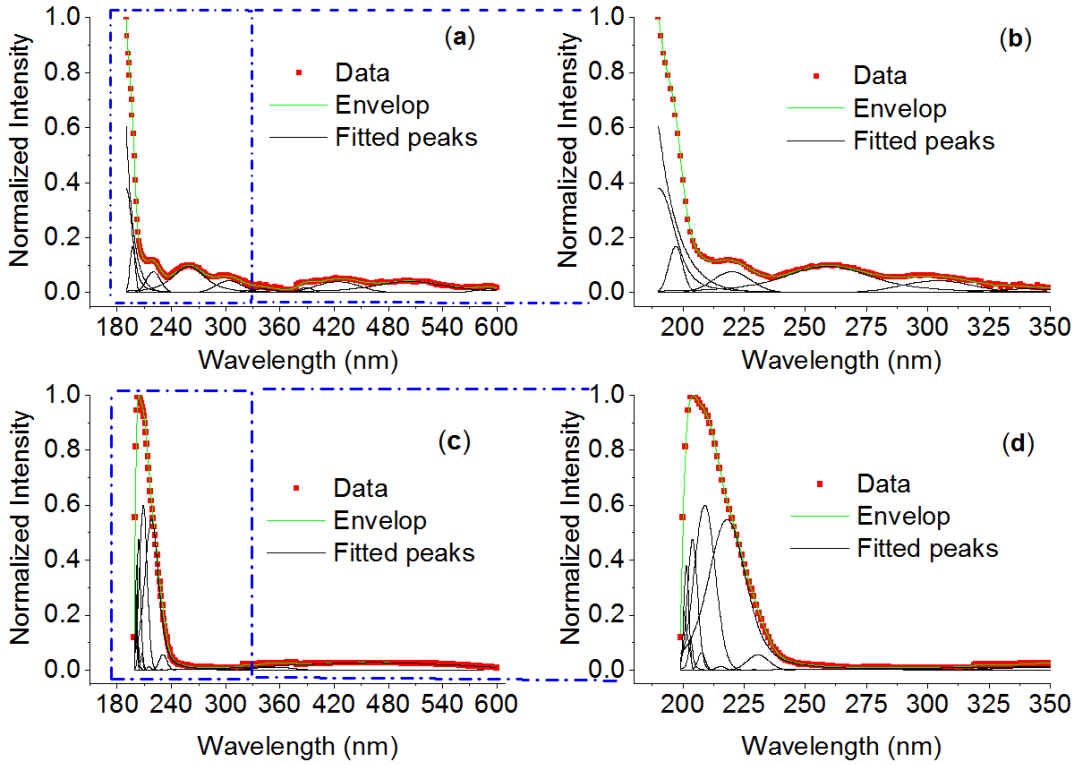

FIGURE 4.3: UV-Vis data for sample washed with (a) water (till 600 nm) (b) water (zoomed till 350 nm) (c) ethanol (till 600 nm) (d) ethanol (zoomed spectrum up to 350 nm).

ethanol washed samples are polydisperse in nature (Chapter 3). So, it can be said from the present data that the NP sizes in water washed sample are smaller than the ethanol washed samples. Further absorption peaks after 260 nm maybe due to very big sized clusters; the intensity of these peaks is low for both samples. Such a low magnitude of these peaks may indicate the availability of few big clusters in the samples. HRTEM studies revealed the existence of such clusters (Figure 4.4).

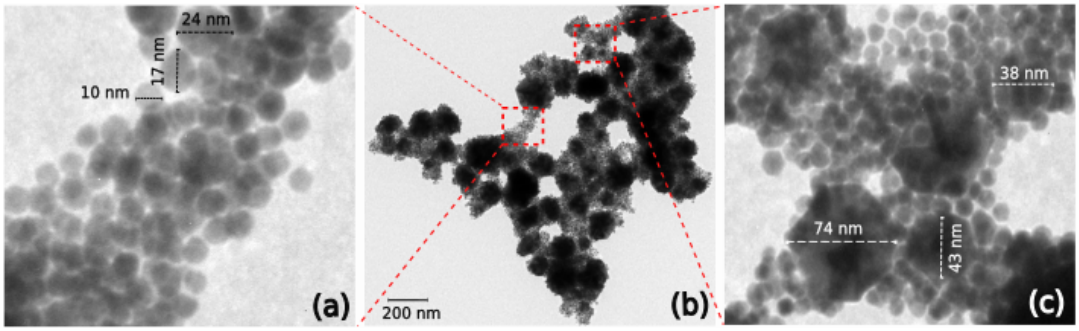

FIGURE 4.4: HRTEM image showing variation in size for Pd NPs washed with ethanol (a) small size (b) all size (c) mixed sizes.

TABLE 4.2: Device baseline resistance

Sample category	Resistance
Water-washed	0.12 - 1.12 MΩ
Ethanol-washed	0.5 - 2.0 kΩ

4.4 HYDROGEN GAS SENSING RESULTS AND DISCUSSION

The water washed and ethanol washed nanoparticles were used to make resistive sensor devices. The methodology for the preparation of resistive sensor devices has been outlined in Chapter 2. The baseline device resistance will be different due to difference in PVP surface coverage and it is obvious that water washed film will have comparatively higher baseline resistance (Table 4.2). This is because water washed nanoparticles have uniform PVP coverage around their surface and so the interparticle barrier is high. Figure 4.5 presents the repeated transient patterns for the two samples at room temperature (RT). The %response magnitudes are different for both samples at room temperature (RT) and high temperature (50^{o}C) [Figure 4.5]. In fact, the %response for the water washed sample is higher than ethanol washed sample and with the increase in temperature the magnitude of %response is decreasing for both categories. These differences in the hydrogen response can be realized with the help of the sensing mechanism [28, 71]. This mechanism has two steps and is discussed in detail in Chapter 3. In the first step, the surface adsorbed oxygen atoms are removed via water formation and in the second step the electronic and geometric effects occur in succession [30, 89]. The variation in the device baseline resistance upon exposure to hydrogen is presented in Figure 4.5a, b & Figure 4.6. Washing of the nanoparticles can affect the sensing process because the PVP coverage on nanoparticle surface is attacked by certain solvents such as ethanol [25]. Hence the surface cleaning of adsorbed oxygen atoms (i.e., the first step in sensing) is likely to be different for the two categories of samples because there is non-uniform PVP coverage in ethanol washed sample and more or less uniform PVP coverage in water washed sample. The difference in coverage can lead to relatively higher atmospheric oxygen contamination to passivate the uncovered active surface sites for the ethanol washed nanoparticles. Therefore, during the first step, the ethanol washed sample will consume more hydrogen atoms to remove its surface adsorbed oxygens while the water

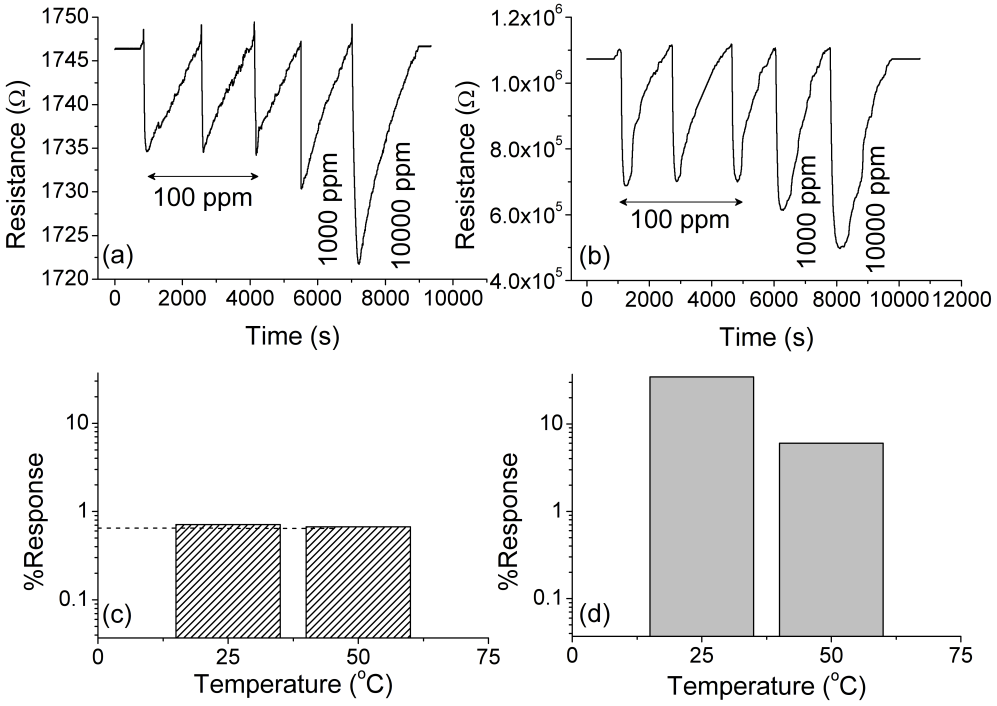

FIGURE 4.5: (a) Transient patterns of ethanol-washed samples at RT in H_2. (b) Transient patterns of water-washed samples at RT in H_2. (c) 100 ppm hydrogen response variation with temperature for ethanol-washed samples. (d) 100 ppm hydrogen response variation with temperature for water-washed samples.

washed samples will consume less for the surface oxygen cleaning. Accordingly, the actual hydrogen adsorption into the palladium will be relatively higher for the water washed sample. So, from this purview the %response of waster washed samples is likely to be higher than ethanol washed samples (Figure 4.5c, d) [3].

A simple Langmuir model is adopted and some simple calculation is done to calculate the equilibrium constants to understand the subtle difference in intensity of hydrogen activity in the first step [33]. According to this model %response ($\Delta R/R$) can be expressed using equation 4.1. Here 'P_{H2}' is the hydrogen concentration and 'κ' is the "equilibrium constant". The variation of 'κ' amongst the samples will indicate the difference in hydrogen activity in the first step.

$$\frac{\Delta R}{R} = \sqrt{\kappa}\sqrt{P_{H2}} \tag{4.1}$$

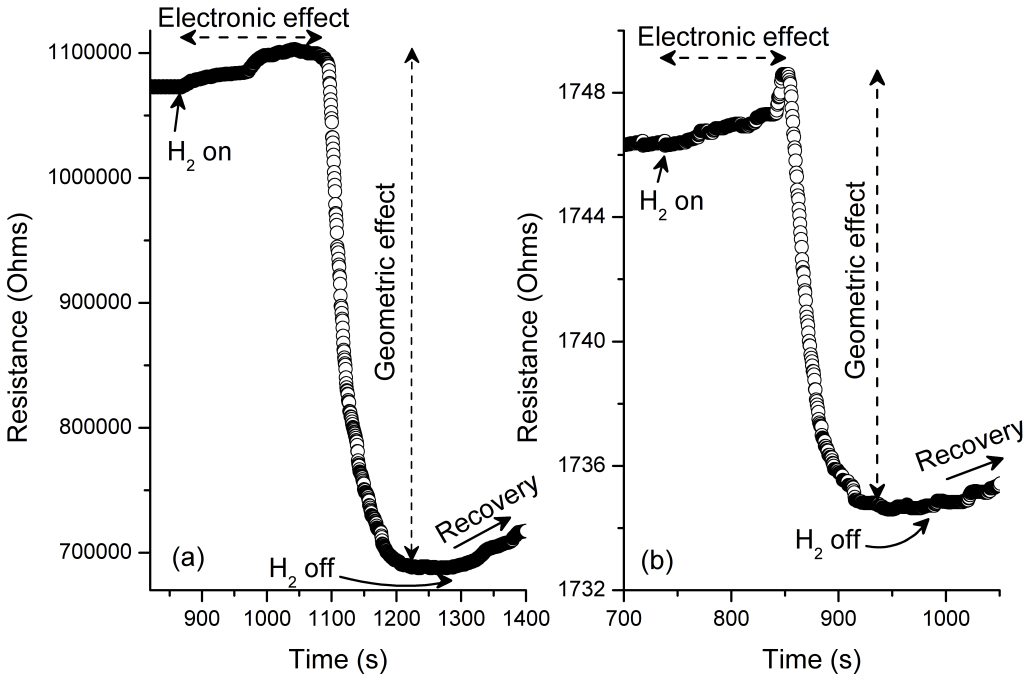

FIGURE 4.6: Sensing effects (electronic and Geometric) for the devices at RT (100 ppm hydrogen) (a) water washed and (b) ethanol washed.

The dissociative hydrogen adsorption can be presented with equations (4.2) & (4.3).

$$H_2 = 2H \quad adsorption \tag{4.2}$$

$$2H = H_2 \quad desorption \tag{4.3}$$

Here 'κ_a' and 'κ_d' are associated as the contants for adsorption and desorption processes, respectively (eq 4.2 & 4.3). The equilibrium constant κ is the ratio of these adsorption and desorption constants. Eq (4.1) is established by doing a linear fit of the experimental data (Figure 4.7). The slope of the straight line fit gives the value of κ. It is observed, activity of sample washed with water is higher than sample washed with ethanol because κ is comparatively larger for water washed sample. The second sensing step includes electronic and geometric effects. The %response is mainly dominated by the geometric response because the change in resistance is high during the geometric effect. Strain analysis with GIXRD result is done to illustrate the difference in the geometric activity (Figure 4.1 & 4.2). The tensile strain is obvious from the positive slope of the plot in both the samples, and this tensile strain

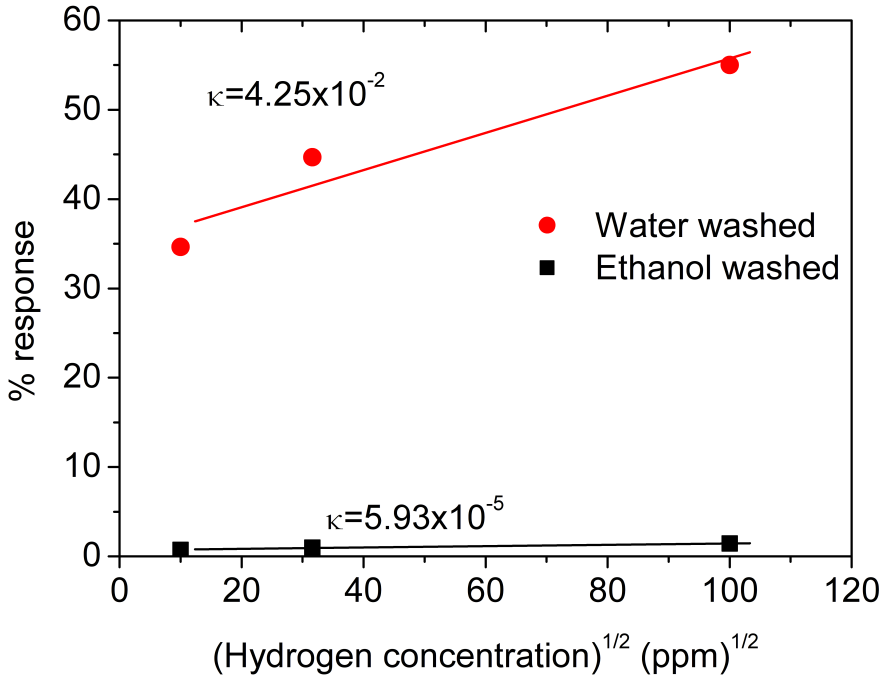

FIGURE 4.7: Equilibrium constant (κ) for Pd nanoparticle washed with water and ethanol.

tunes the geometric effect. So, if the magnitude of this tensile strain is high, the geometric effect gets accelerated. For compressive strain, the opposite effect is there. Since samples washed with water has larger magnitude of tensile strain (than samples washed with ethanol), the intensity of geometric effect is comparatively better in water washed sensor devices. So, considering the hydrogen activity in first and second steps it can stated that the %response in water washed samples will always be higher than the other category (Figure 4.5). The deterioration of %response with the increase in temperature may be attributed to the dominance of hydrogen desorption over adsorption (Figure 4.5).

The effect of humidity on the %response was also tested because un-desorbed water molecules can block active sites. In the sensing mechanism the water formation is justified. Hence ambient moisture as well as insitu generated water can accumulate on the nanoparticle surface because PVP has a strong affinity for water molecules [86]. So, low PVP coverage will gather relatively less moisture molecules. Hence, the %response of water washed samples can deteriorate when ambient humidity increases (Table 4.3). The calculated response time can also be affected due to increase in concentration of moisture molecules. This can delay the device saturation time,

TABLE 4.3: Effect of moisture on the device parameters (in 100 ppm H_2) at RT

	Water washed		**Ethanol washed**	
Humidity %	**% response**	**Response time (s)**	**% response**	**Response time (s)**
55	37.09	57.5	0.76	40.7
65	28.57	70.5	0.71	45.5

which can account for the rise in response time when ambient humidity increases. The recovery is slow ($\sim$ minutes) in both the samples, and this can be attributed to reasons such as slow recovery of strained lattice, trapping of hydrogen in bulk of palladium, presence of moisture, *etc*.

4.5 SUMMARY

This work illustrates the influence of washing agent on the performance of palladium nanoparticles in hydrogen ambient. Different washing agents will have different effect and in this study water and ethanol have been selected. The role of washing agent is to tune the stabilizer coverage on the nanoparticle surface. Such a control helps to bring difference in hydrogen activity of the palladium nanoparticles.

Chapter 5

Influence of stabilizer molecular weight on inter-nanoparticle surface barriers and the hydrogen response pattern of resistive hydrogen sensors

When palladium particles are exposed to hydrogen, the temporary formation of palladium hydride and the subsequent volume expansion of the palladium lattice play vital roles. Palladium hydride exists in two phases *viz.*, α-phase (low hydrogen content) and β-phase (high hydrogen content) [28, 46, 53]. The initial hydride formation leads to increase in resistivity of palladium. Hence a device made with palladium nanoparticles shows initial increase in device resistance due to the formation of palladium hydride. This is called electronic effect. Subsequently the volume of the palladium nanoparticles increases, which leads to decrease in device resistance. These effects of increase and decrease in device resistance are coupled to each other and occur in succession. Hence it is difficult to isolate each of these effects.

PVP acts as a stabilizer and resides on the surface of the nanoparticles. PVP prevents the agglomeration and it is reported that post nanoparticle synthesis, the PVP-particle bonding is not broken [57]. When films are formed using these nanoparticles, these PVP branches normally act as an interparticle barrier. The amount of PVP that resides on a nanoparticle surface is dependent on the availability of PVP during nucleation/growth, which in turn is dependent on starting amount of PVP. So, if the

starting concentration of PVP is varied, it likely that the PVP surface coverage can be tuned. There is one other factor i.e., the PVP molecular weight, which can also affect the surface distribution of PVP. Basically if the molecular weight is high, it means the PVP chains are relatively bulkier. Such complicated chains if used in low concentration can provide a non-uniform surface coverage on the nanoparticle surface during synthesis. Hence, after film preparation, the interparticle barrier may be negligible in such cases. However, if the starting concentration is high, interparticle barrier may be uniform.

In this chapter, a bulky PVP (Mw 40000) concentration is varied to illustrate the difference in hydrogen sensing performance. HRTEM and XRD material characterization results have been included in this chapter. A suitable sensing mechanism is also presented to understand the role of interparticle barrier.

5.1 CHARACTERIZATION

The verification of the nanoparticle yield using parameters such as size, shape and crystallinity were done using HRTEM and XRD. The grazing incidence angle for XRD was $\sim$2.5 degrees. The detector was moved between 5 & 80 degrees. The whole experiment was performed at room temperature and the data is presented in Figure 5.1. Sharp peaks corresponding to (111), (200) and (220) indicate for the formation of FCC palladium nanoparticles. HRTEM results revealed that the palladium nanoparticles were more or less spherical in shape. The three samples corresponding to the three concentrations (0%, 20%, and 32% PVP) resulted in 50.68 nm, 11.73 nm, and 12.71 nm sized particles, respectively (Figure 5.2). The large clusters in the 20% sample are due to the low PVP concentration and such clusters are relatively less in the 32% sample. The 0% sample only shows agglomerated clusters. The absence of PVP (0% PVP) will give irregular shaped particles with very large size.

5.2 HYDROGEN GAS SENSING

The hydrogen sensor study was conducted in the temperature range room temperature (RT) to 60^{o}C. The sensing data is presented in Figures 5.3 & 5.4. The 0% PVP samples were insensitive to hydrogen. When the 20% PVP sample was exposed to

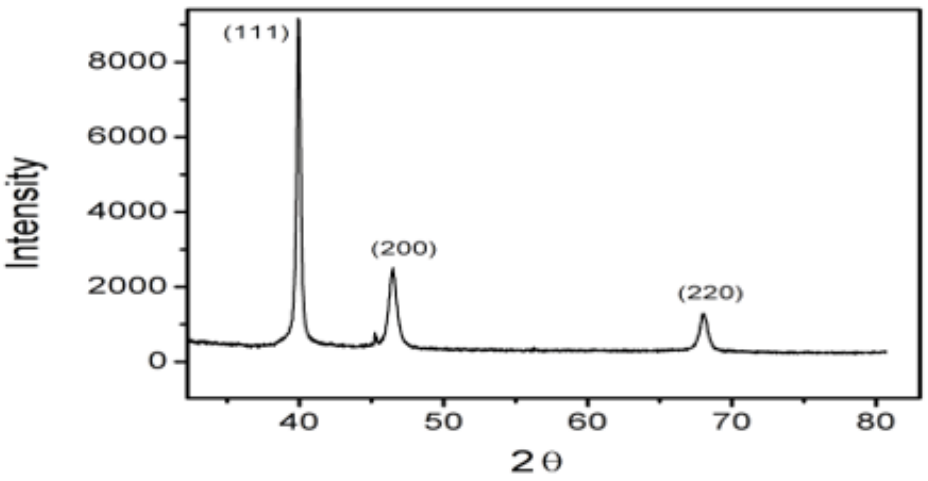

FIGURE 5.1: GIXRD of Pd nanoparticles synthesized with PVP (Mw 40000).

TABLE 5.1: Nature of response and magnitude of the parameters in 100 ppm hydrogen at RT

PVP %	Response type	Response %	Response time (s)
0	Nil response	—	—
20	Electronic	3.38	32
32	Electronic & Geometric	3.26	51

hydrogen gas, only increase in resistance was observed. However, for the 32% sample both increase and decrease in device resistance was observed upon exposure to hydrogen. When the hydrogen gas flow was discontinued, the device resistance slowly recovered back to its baseline value. The performance of 20% PVP and 32% PVP samples was excellent at room temperature and for higher temperatures (40^oC, 50^oC and 60^oC), the hydrogen response deteriorated. Basically, this high temperature deterioration was mainly observed in the device recovery because the devices showed either partial recovery or was unable to recover. The response parameters are tabulated in Table 5.1. The parameters were calculated in the same manner as mentioned in Chapter 3. During measurements, the relative humidity was 30% ($\pm$3%). The solid gas interaction is presented in Figure 5.5. The hydrogen molecules are adsorbed by the palladium and few important changes occur in the nanoparticles. During the initial interaction of hydrogen with the catalytic palladium surface, the surface adsorbed oxygen atoms are removed and then hydrogen is adsorbed by

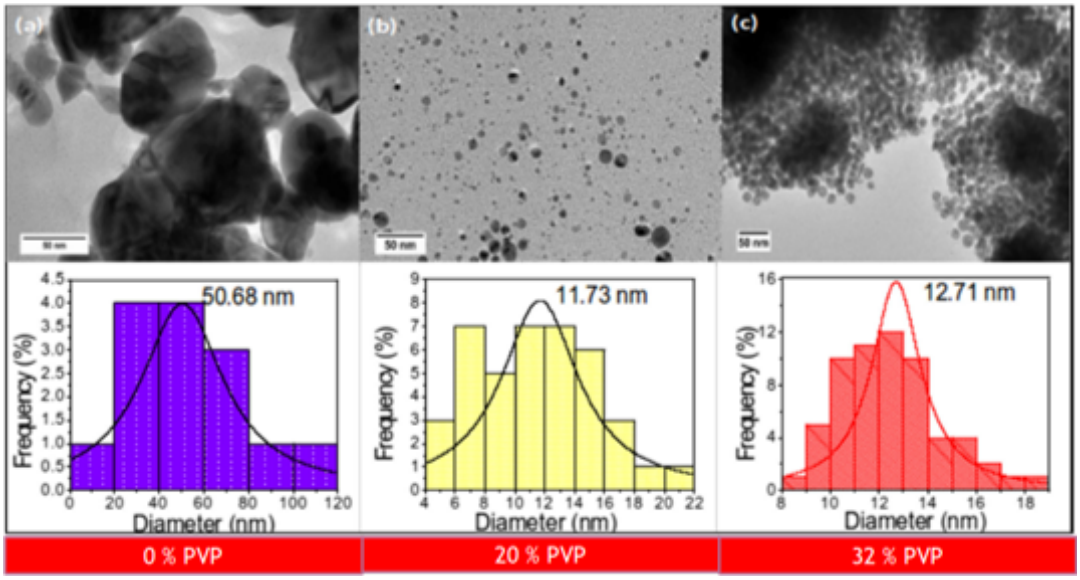

FIGURE 5.2: HRTEM of Pd nanoparticles synthesized with PVP (Mw 40000) (a) 0% PVP (b) 20% PVP (c) 32% PVP.

palladium (eq-5.1). From these equations it is clear that palladium has no sensitivity for moisture [34]. However, if moisture is unable to desorb from the palladium surface, the hydrogen response is affected. Hence the relative humidity of the ambient atmosphere can create some moisture desorption issues. Of course, the dynamic flow of carrier gases during sensing reduces the chance of moisture accumulation in the system.

$$\frac{1}{2}O_2 + 2e^{-1} \xrightarrow{Pd} O^{-2} \tag{5.1a}$$

$$H_2 \xrightarrow{Pd} 2H^{+1} + 2e^{-1} \tag{5.1b}$$

$$2H^{+1} + O^{-2} \xrightarrow{Pd} H_2O \tag{5.1c}$$

$$H_2 + \frac{1}{2}O_2 \xrightarrow{Pd} H_2O \tag{5.1d}$$

Now the palladium nanoparticle surface is rich in hydrogen and non-stoichiometric palladium hydride (PdH_y) is formed. The formation of hydride leads to the initiation of electronic and geometric effects in the sensing palladium nanofilm, and these effects have been discussed in Chapter 3. In this study the inter-nanoparticle barrier due to the surface coverage of PVP is found to influence the nature of hydrogen sensing. For instance, if PVP coverage is non-uniform, there is high chance that two consecutive nanoparticles can touch each other and thus have negligible inter-particle barrier. The extent of this PVP occupancy on particle surface is dependent

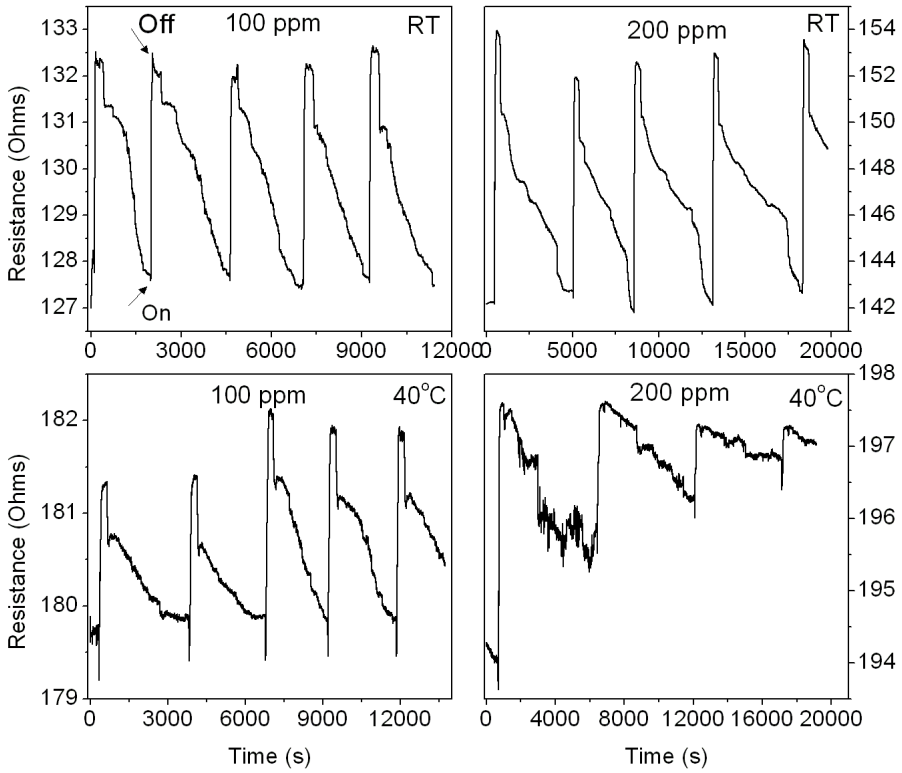

FIGURE 5.3: The gas (hydrogen) response of 20% PVP sample.

on the amount of PVP used during synthesis to a large extent, and to a relatively lesser extent on the bulky nature of PVP (i.e., molecular weight). For this chapter, a heavy molecular weight (∼40,000) PVP is used. Hence the PVP entanglement on palladium surface is likely to be erratic due to the bulky nature of the PVP chains. Moreover, if the concentration of PVP is varied, the surface coverage can further be controlled. In fact, this study has two categories of samples *viz.*, 20% & 32% samples. Therefore, the 32% sample is expected to have better PVP barrier with respect to the 20% sample.

During sensing, the 32% sample responded to hydrogen by manifesting initial increase (electronic effect) and subsequent decrease (geometric effect) in device resistance, while the 20% sample revealed only the initial rise in resistance. Earlier in Chapter 3, the gas response of palladium nanoparticles [having low molecular weight (∼8,000) PVP coverage] showed both electronic and geometric effects in all sample categories synthesized by varying PVP concentration from 20% to 60%. This interesting difference is arising solely due to the PVP molecular weight. Here in this chapter the PVP with molecular weight (∼40,000) is probably distributed on

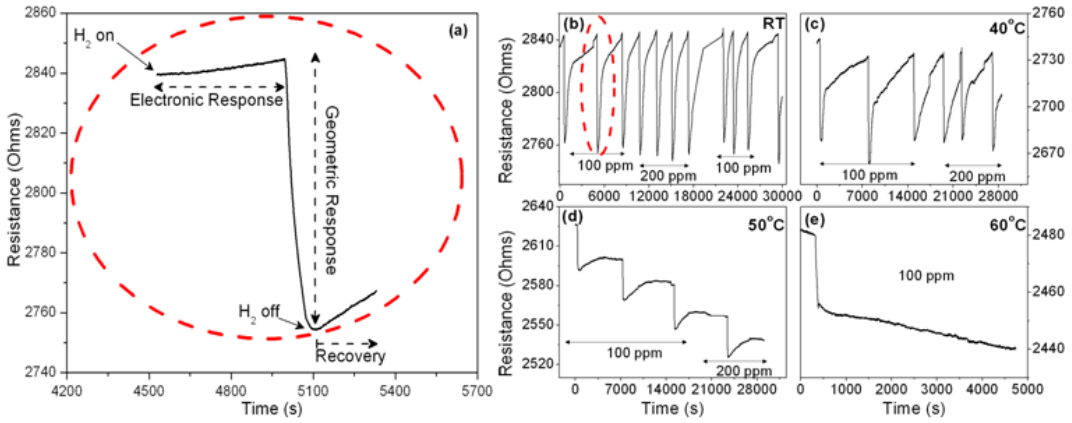

FIGURE 5.4: The gas (hydrogen) response of 32% PVP sample (a) response highlight the initial increase (electronic response) and the subsequent decrease (geometric response) followed by recovery (b) room temperature (RT) (c) 40^{o}C (d) 50^{o}C (e) 60^{o}C.

nanoparticle surface in such a manner that it renders dense and scarce PVP barrier in 32% and 20% samples, respectively. Basically, nature of the barrier (i.e., dense or scarce) is directly realized from the magnitude of the baseline device resistance of the sensing devices. The device made with 32% sample showed baseline resistance in the range 1.7 – 2.8 kohms, while the device made with 20% sample showed only 127 ohms. Such a variation in interparticle barrier can also imply that the interparticle gap is relatively larger in 32% sample. The fact of the matter is this interparticle gap (or barrier) controls device resistance change during the volumetric expansion (or geometric effect) of the nanoparticles. If the gap is large, the geometric effect is significant; while if the gap is negligible, geometric effect is insignificant. As shown in the sensing mechanism (Figure 5.5), the palladium nanoparticles in the 32% sample have good PVP coverage that results in appreciable interparticle gap. This gap reduces when the nanoparticles undergo volumetric expansion upon hydrogen adsorption, and it likely that some of the particles can come in contact with neighbouring particles during this expansion. Accordingly, the resistance of the device falls drastically after the initial increase in 32% sample. However, for the 20% sample, the particles are very close to each other. Hence even if there is volumetric expansion of the nanoparticles, drastic decrease in device resistance does not occur.

In the 0% PVP sample, there is no PVP coverage during synthesis. So, particles agglomerate at random during synthesis. Further in the devices made with these agglomerated clusters, the current paths are all shorted. So, occurrence of electronic

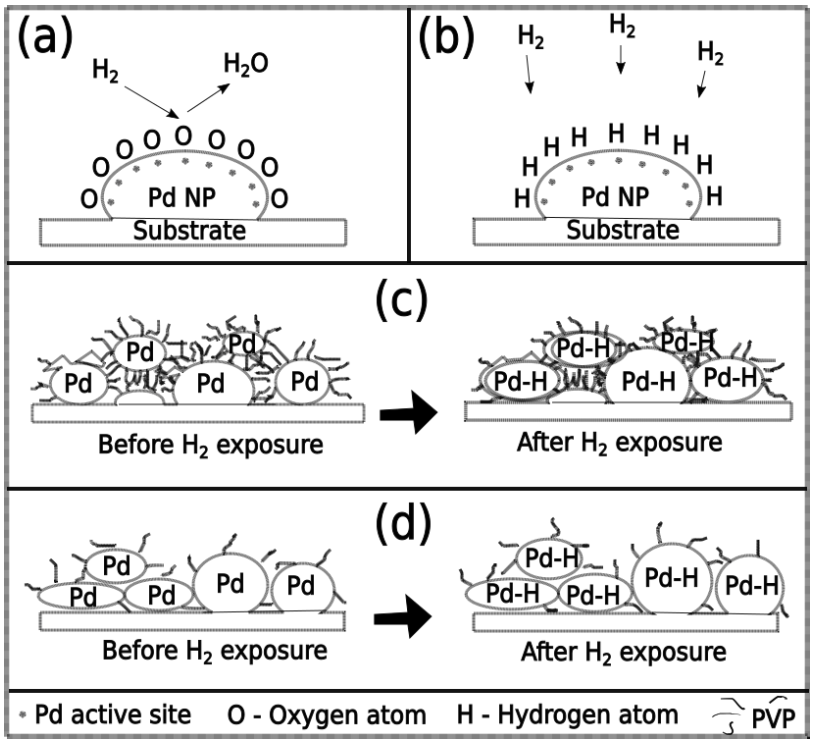

FIGURE 5.5: The gas sensing mechanism: (a) water formation (b) hydrogen adsorption and formation of PdH_y (c) 32% sample showing dense PVP barrier around each nanoparticle and large interparticle gap that decreases in presence of hydrogen (d) 20% sample showing scarce interparticle PVP barrier in absence of hydrogen.

and geometric effects is not possible. For the 20% and 32% samples, the room temperature performance is best. At high temperatures, the performance is deteriorating. This can be attributed to the hydrogen desorption from the particle surface and thermal expansion of the metallic nanoparticles.

5.3 CONCLUSION

Palladium nanoparticles synthesized with high molecular weight PVP can impart different baseline resistance in simple resistive devices. Such difference in baseline resistance is due to the variation in the interparticle barrier, which has a profound impact on the nature of hydrogen response. Separate manifestation of the electronic effect was observed for samples have low interparticle barrier, while dual manifestation of electronic and geometric effects was observed with relatively larger PVP barrier. The high recovery time is probably due to slow release of hydrogen from the samples. Also, the synthesized nanoparticles are suitable for room temperature application.

Chapter 6

Catalytic nanoparticle purity (extent of hydrogen contamination) and resistive device stability

The lifespan of gas sensing devices prepared with catalytic materials such as palladium is reduced by catalytic poisoning. Basically, the repeated use of a catalytic material for gas adsorption/desorption purpose can lead to some permanent chemical reactions, which will ultimately deteriorate the catalytic properties of the material. This is aggravated if the device operating temperature is high because at elevated temperature, some permanent chemical changes in a material is likely. Palladium is an interesting catalytic material and is an excellent hydrogen adsorber. Palladium nanoparticles (solid) interact with the hydrogen (gas) atoms on their surface during gas sensing. The hydrogen-palladium solid solution is formed and slowly palladium hydride (PdH_y) is also formed [56]. For a maximum value of $y \sim 0.015$, the "α-phase" of palladium hydride is predominant, and the conversion to the "β-PdH_y" happens in the range $0.015<y<0.7$ [53]. This β-hydride is a permanent material conversion and creates problems such as incomplete device recovery. Hence if palladium is slowly converted to β-PdH_y its catalytic property will be reduced.

Stable device performance is also affected if there is deterioration of the baseline resistance. The stable baseline resistance can vary due to many reasons such as catalytic poisoning, mechanical deterioration of the sensing film, excessive moisture adsorption, *etc.* In palladium nanoparticle based resistive devices, these factors can affect the response parameters. Hence studies are necessary to cross check whether material purity is intact after repeated use and the device performance is more or less stable after prolonged usage.

In this chapter, x-ray diffraction (XRD) based strain analysis and very long period sensing studies are presented in order to establish the fact that palladium nanoparticle based resistive devices are suitable for long term room temperature operation.

6.1 STRAIN ANALYSIS

For this analysis, two category of palladium nanoparticle (NP) based films were selected. The first category of films is based on as prepared palladium nanoparticles; for the second category the as prepared films were repeatedly tested in hydrogen ambient in the temperature range RT – 60°C. Both these films were studied by XRD and the results are shown in Figure 6.1. The three important peaks corresponding to the planes (111), (200), and (220) are observed in both the XRD pattern. The peaks in both patterns are slightly displaced with respect to each other. The strain analysis

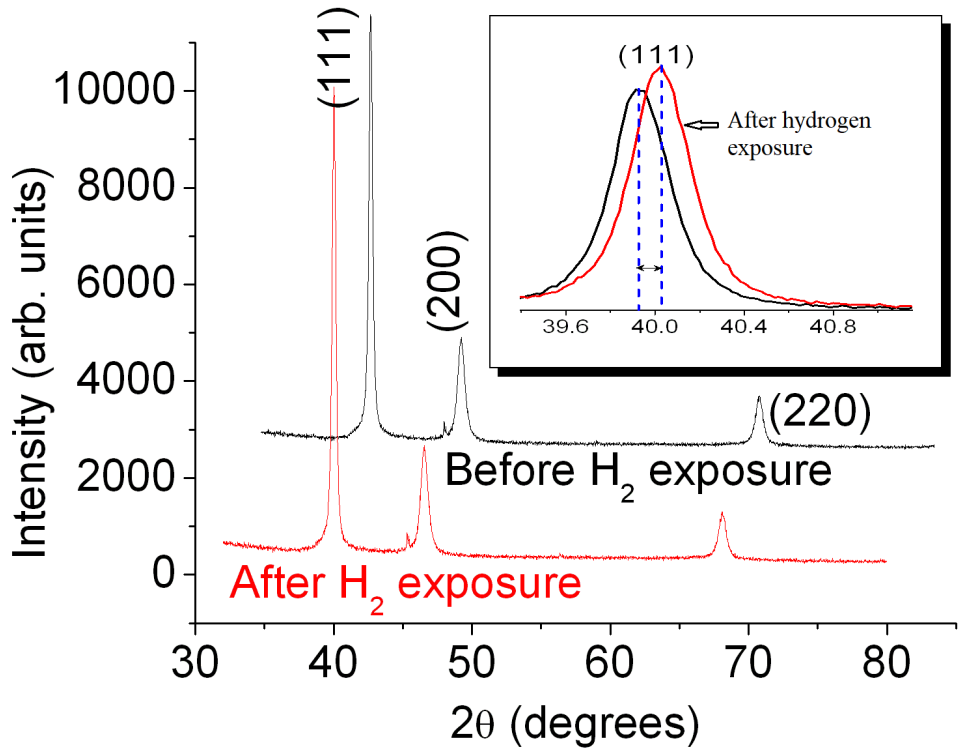

FIGURE 6.1: XRD graph of films based on Pd NPs (synthesized with 32% PVP) before and after hydrogen exposure.

is done by plotting a graph between '$\beta \cos\theta$' and '$\sin\theta$'. Here 'β' refers to the width (line broadening) of the peak located at a particular 2θ [87, 93]. For three peaks, three experimental data points are plotted and a best linear fit is done (Figure 6.2). The

slope of this fitted straight line gives the strain of the material. The strain values are "0.01005 and 0.01008" corresponding to "before and after" hydrogen exposure. A very small change in strain is observed and this cannot be attributed to palladium hydride formation. This is due to the fact that upon hydride formation the inter-planar spacing will increase and the 2θ position will shift towards relatively lower angle [38]. However, here we observe that the "After H_2 exposure" data in Figure 6.1 is showing shift in (111) peak towards high angle side. Therefore, this negligible difference in strain maybe due to the repeated volumetric expansion (geometric effect) undergone by the palladium lattice during hydrogen sensing. Basically, strain is a result of disorder and chaos in the periodic palladium lattice. The geometric effect to some extent is responsible for defect migration in the particles. This leads to the slight increase in the particle strain in the films after hydrogen exposure. Hence the above result support the fact that palladium nanoparticle system is not contaminated after repeated use in hydrogen ambient.

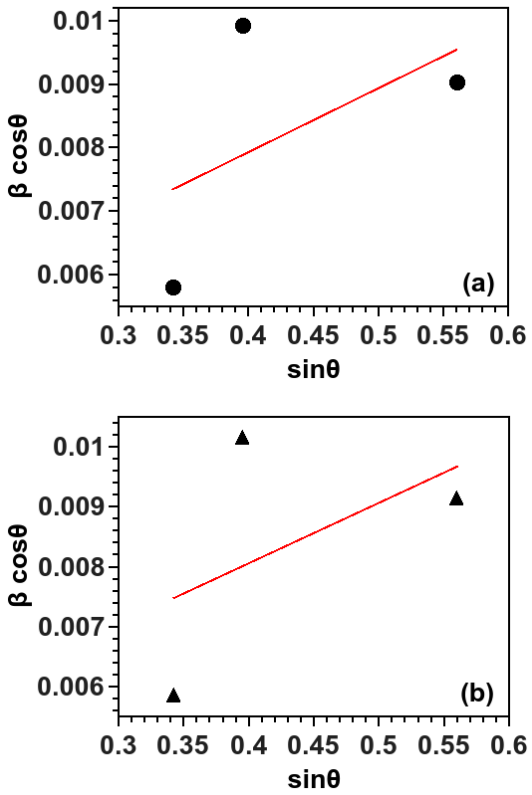

FIGURE 6.2: W-H plot for thin films prepared with Pd NPs synthesized with 32% PVP (Mw $\sim$ 40,000): (a) films before hydrogen exposure (b) films after repeatedly testing in hydrogen ambient in the temperature range RT - 60^{o}C.

6.2 DEVICE STABILITY STUDY

The resistive devices were exposed repeatedly to hydrogen "ON/OFF cycles" for the long-term stability study at room temperature. The data for a sample is shown in Figure 6.3. During this study the hydrogen "ON/OFF cycles" were applied for a continuous period of 12-hrs per day. Thereafter, the next day the same procedure was continued for another 6-days. The device response is stable and %response is showing an appreciable stable value with little deviation (Figure 6.3). Hence it is apparent that the palladium nanoparticle films developed by the drop casting technique are quite suitable for repeated use in gas sensors.

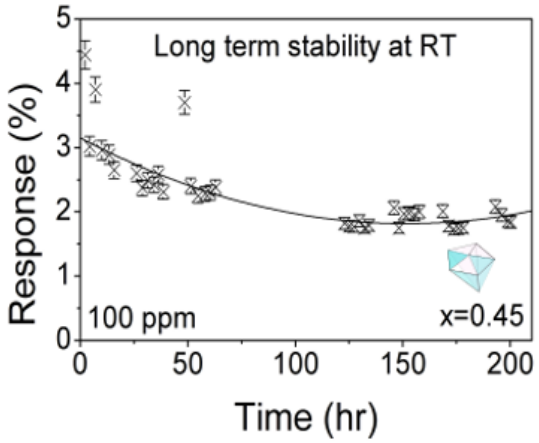

FIGURE 6.3: Long term stability at RT for devices based on palladium nanoparticle synthesized with precursor - PVP (Mw 8000) ratio= x = 0.45.

6.3 CONCLUSION

The above study was undertaken to clarify few facts: firstly, the catalytic contamination during palladium-hydrogen interaction; secondly the long-term device stability. It was observed that the palladium nanoparticle film is not poisoned by repeated use in hydrogen in the temperature range RT-60°C. Moreover, the device performance for a very long usage period ($\sim$ 200 h) is quite satisfactory. Furthermore, the devices showed excellent long-term stability after a gap of 30 days from initial testing.

Chapter 7

Summary, conclusions and future scope

7.1 SUMMARY

Pd Nanoparticles having PVP coverage were synthesized by conventional Polyol method and synthesis parametric variation was implemented with respect to one parameter i.e., stabilizer (PVP) concentration. The other synthesis parameters such as temperature, reagents amounts, pH of the solution, *etc.*, were not altered within the limits of experimental accuracy. The crystallinity, morphology & the hydrogen response of the nano yield was analyzed with experimental data. In the nano scale, the factors that control device performance are particle size, shape, dispersity, and other film properties. Additionally material contamination with repeated usage and the resistive device performance stability were also studied.

The optimization of PVP concentration was done by (i) varying PVP to precursor ratio, (ii) changing the molecular weight of PVP (8,000 and 40,000) and (iii) using different washing agents. The PVP quantity variation during synthesis was achieved by technique (i). HRTEM results show the shape and size variation with changing PVP to precursor ratio. GAXRD confirmed the formation of polycrystalline Pd nanoparticles which was also supported by SAED pattern. All these material characterization results were correlated with the corresponding hydrogen sensor response. The resistive device response changed with the change in shape & size of the nanoparticles. An optimum in the hydrogen sensing was observed for small sized palladium nanoparticles having octahedron or decahedron shapes. The variation of dispersity of the nanoyield reveals that a large value of polydispersity index provides multiple sensing channels in the thin films, which is the cause for excellent

hydrogen response.

The molecular weight variation as mentioned in (ii) was implemented to understand the control of this synthesis parameter (PVP) on the nature of hydrogen response. A relatively larger molecular weight (40,000 Mw) when used in small quantities during synthesis is unable to provide a high barrier/gap between the nanoparticles. As a result only electronic hydrogen response was observed. However when high quantities of large molecular weight PVP was used the barrier/gap increased, and both electronic and geometric responses were observed.

The PVP quantity variation after synthesis was achieved by technique (iii). The effect of washing agents on the polymeric surface coverage of palladium nanoparticles was verified by GAXRD and hydrogen sensor studies. Solvent such as ethanol can attack the PVP-palladium attachment and this can lead to the elimination of PVP during repeated washing. However, water has negligible effect on the PVP-palladium bonding. Such elimination of PVP by washing solvent from the palladium nanoparticle surface can lead to blockage of available active sites by native oxygen impurities during film preparation. Hence the hydrogen response parameter for water washed palladium nanoparticles is better than ethanol washed samples.

GAXRD data analysis (strain calculation) was performed before after hydrogen sensing to confirm the catalytic purity of sensing films. Negligible change in strain ensures negligible contamination of the sensing material due to repeated exposure to hydrogen. Also the device stability with time was confirmed by testing the response of devices for a very long period. Sensing mechanisms for all case studies have been proposed and critically analysed with respect to the hydrogen gas sensing data.

7.2 CONCLUSIONS

It is apparent from the results that large palladium chunks have no role in hydrogen sensing and the PVP amount has an important role in giving proper shape to palladium particles. Moreover the palladium-hydrogen interaction can be correlated to particle morphology. This study indicates that the material is suited for room temperature application in the field of hydrogen sensors. Specifically, the studies reveal that PVP (Mw 8000) % = 32 - 45% (with respect to precursor amount) is the suitable range for low temperature applications, while PVP% = 20% is good for elevated

temperature applications. Further, if the surface coverage is varied with different washing solvent, the catalytic activity can also be varied. Interestingly, the PVP surface coverage can increase the device resistance and change the type of hydrogen sensing pattern (if its molecular weight is increased). This enables the separation of the "electronic effect" to a large extent. The studies also reveal that relative humidity can affect the response of sensors based on PVP covered palladium nanoparticles. Moreover, XRD data revealed that these Pd NP based devices can be used for a long time period because there is negligible change in strain before and after hydrogen sensing.

7.3 FUTURE SCOPE

In this study, the response and recovery times are high. So, the ways of improvement of these times must be evaluated by initiating further modification of the experimental parameters. The scope of this work can also be improved, if the synthesis technique and film properties are changed. A new synthesis approach can also impart better film stability to give relatively better room & high temperature sensor performance. The contamination from real field atmosphere was studied by GAXRD and hydrogen response. However, accurate determination of surface impurities can be done by adopting in situ spectroscopic studies (such as X-ray photoelectron spectroscopy). Such a study can quantify the nanoparticle surface oxygen impurities. Additionally selective response of palladium nanoparticles towards other gases may be pursued. Due to experimental limitations these studies were not pursued in the current work.

Bibliography

[1] Sarah M Adams et al. "Non-lithographic SERS substrates: tailoring surface chemistry for Au nanoparticle cluster assembly". In: *Small* 8.14 (2012), pp. 2239–2249. URL: doi:10.1002/smll.201102708.

[2] A. Aitken and M.P. Learmonth. "Protein Determination by UV Absorption. In J.M Walker (eds) The Protein Protocols Handbook". In: Springer Protocols Handbooks. Humana Press, 2002. Chap. 1.

[3] Pooja Bhardwaj, Partha Bir Barman, and Surajit Kumar Hazra. "Hydrogen response of palladium nanoparticles washed with different solvents". In: *Bull Mater Sci* 44.45 (2021). URL: https://doi.org/10.1007/s12034-020-02323-z.

[4] Pooja Bhardwaj, Partha Bir Barman, and Surajit Kumar Hazra. "Shape dependent hydrogen response in palladium nanoparticle based sensors". In: *Materials Today: Proceedings* 28 (2020), pp. 218–222.

[5] Pooja Bhardwaj, P.B. Barman, and S.K. Hazra. "Effect of Capping-Agent Concentration on Size and Size Dispersity of Palladium Nanoparticles for Resistive-Type Hydrogen Sensors". In: *Journal of Electronic Materials* 49.11 (2020), pp. 6656–6670. URL: DOI10.1007/s11664-020-08431-0.

[6] Beant Kaur Billing, Prabhat K. Agnihotri, and Narinder Singh. "Fabrication of branched nanostructures for CNT @ Ag nano-hybrids: application in CO2 gas detection". In: *J. Mater. Chem. C* 5.17 (2017), pp. 4226–4235.

[7] S.J. Budijono et al. "Block copolymer surface coverage on nanoparticles". In: *Colloids and Surfaces A: Physicochemical and Engineering Aspects* 360.1–3 (2010), pp. 105–110. URL: https://doi.org/10.1016/j.colsurfa.2010.02.016.

[8] Ilaria Calabrese et al. "Deconvolution procedure of the UV–vis spectra. A powerful tool for the estimation of the binding of a model drug to specific solubilisation loci of bio-compatible aqueous surfactant-forming micelle". In: *Spectrochimica Acta Part A: Molecular and Biomolecular Spectroscopy* 142.5 (2015), pp. 150–158.

[9] G Cao. *Nanostructures and Nanomaterials*. Imperial College Press, 2004.

[10] Claudia C. Cassol et al. "The role of Pd nanoparticles in ionic liquid in the Heck reaction". In: *Journal of the American Chemical Society* 127.10 (2005), pp. 3298–3299.

[11] [T. Chen et al. "Single-molecule nanocatalysis reveals facet-dependent catalytic kinetics and dynamics of palladium nanoparticles". In: *ACS Catal.* 7.4 (2017), pp. 2967–2972.

[12] Soshan Cheong, John D. Watt, and Richard D. Tilley. "Shape control of platinum and palladium nanoparticles for catalysis". In: *Nanoscale* 2.10 (2010), pp. 2045–2053.

[13] Tae Joon Cho et al. "Unexpected Changes in Functionality and Surface Coverage for Au Nanoparticle PEI Conjugates: Implications for Stability and Efficacy in Biological Systems". In: *Langmuir* 31.27 (2015), pp. 7673–7683.

[14] M.G. Chung et al. "Flexible hydrogen sensors using graphene with palladium nanoparticle decoration". In: *Sens Actuators B* 169 (2012), pp. 387–392.

[15] Min Gyun Chung et al. "Flexible hydrogen sensors using graphene with palladium nanoparticle decoration". In: *Sens Actuators B* 169 (2012), pp. 387–392.

[16] Micaela Crespo-Quesada et al. "Structure sensitivity of alkynol hydrogenation on shape-and size-controlled palladium nanocrystals: which sites are most active and selective?" In: *Journal of the American Chemical Society* 133.32 (2011), pp. 12787–12794.

[17] H. Dong, Y-C. Chen, and C. Feldmann. "Polyol synthesis of nanoparticles: status and options regarding metals, oxides, chalcogenides, and non-metal elements". In: *Green Chemistry* 17.8 (2015), pp. 4107–4132.

[18] F Fievet et al. "Homogeneous and heterogeneous nucleations in the polyol process for the preparation of micron and submicron size metal particles". In: *Solid State Ion* 32-33.1 (1989), pp. 198–205.

[19] Fernand Fiévet and Roberta Brayner. "Nanomaterials: A Danger or a Promise?" In: Springer-Verlag, London, 2013. Chap. 1.

[20] B. Fleury et al. "Gold nanoparticle internal structure and symmetry probed by unified small-angle X-ray scattering and X-ray diffraction coupled with molecular dynamics analysis". In: *Nano Lett.* 15.9 (2015), pp. 6088–6094.

[21] Marion E. Franke, Tobias J. Koplin, and Ulrich Simon. "Metal and metal oxide nanoparticles in chemiresistors: does the nanoscale matter?" In: *Small* 2.1 (2006), pp. 36–50.

[22] Lin Gan et al. "Lattice Strain Distributions in Individual Dealloyed Pt-Fe Catalyst Nanoparticles". In: *J. Phys. Chem. Lett.* 3.7 (2012), pp. 934–938. URL: https://doi.org/10.1021/jz300192b.

[23] G. Ghosh et al. "Synthesis and characterization of PVP-encapsulated ZnS nanoparticles". In: *Opt. Mater.* 28.8–9 (2006), pp. 1047–1053.

[24] Sourov Ghosh and C. Retna Raj. "Shape-controlled synthesis of Pt nanostructures and evaluation of catalytic and electrocatalytic performance". In: *Catalysis Science & Technology* 3.4 (2013), pp. 1078–1085.

[25] P. C. Griffiths et al. "Effect of Ethanol on the Interaction between Poly (vinyl pyrrolidone) and Sodium Dodecyl Sulfate". In: *Langmuir* 20.16 (2004), pp. 6904–6913. URL: https://doi.org/10.1021/la049348o.

[26] Peter Grundler. *Chemical Sensors An Introduction for Scientists and Engineers*. 1–2. Springer, Berlin, Heidelberg, 2007.

[27] H. Gu, Z. Wang, and Y. Hu. "Hydrogen Gas Sensors Based on Semiconductor Oxide Nanostructures". In: *Sensors* 12 (2012), pp. 5517–5550. URL: https://doi.org/10.3390/s120505517.

[28] D. Gupta et al. "A low temperature hydrogen sensor based on palladium nanoparticles". In: *Sens Actuators B* 196 (2014), pp. 215–222.

[29] D. Gupta et al. "Temperature dependent dual hydrogen sensor response of Pd nanoparticle decorated Al doped ZnO surfaces". In: *J. Appl. Phys.* 118.16 (2015), p. 164501.

[30] R Gupta, AA Sagade, and GU Kulkarni. "A low cost optical hydrogen sensing device using nanocrystalline Pd grating". In: *International Journal of Hydrogen Energy* 37.11 (2012), pp. 9443–9449.

[31] Hossam Haick. "Chemical sensors based on molecularly modified metallic nanoparticles". In: *Journal of Physics D: Applied Physics* 40.23 (2007), p. 7173.

[32] R. Van Hardeveld and F. Hartog. "The statistics of surface atoms and surface sites on metal crystals". In: *Surface Science* 15.2 (1969), pp. 189–230.

[33] Kamrul Hassan and Gwiy-Sang Chung. "Catalytically activated quantum-size Pt/Pd bimetallic core–shell nanoparticles decorated on ZnO nanorod clusters for accelerated hydrogen gas detection". In: *Sens Actuators B* 239 (), pp. 824–833. URL: https://doi.org/10.1016/j.snb.2016.08.084.

[34] Nilay Hazari, Patrick R. Melvin, and Megan Mohadjer Beromi. "Well-defined nickel and palladium precatalysts for cross-coupling". In: *Nat Rev Chem 1, 0025 (2017).* 1.0025 (2017). URL: https://doi.org/10.1038/s41570-017-0025.

[35] H. Hei et al. "Controlled Synthesis and Characterization of Nobel Metal Nanoparticles". In: *Soft Nanosci. Lett.* 2.3 (2012), p. 34. URL: doi.org/10.4236/snl.2012.23007.

[36] [T. Hubert et al. "Hydrogen sensors–a review". In: *Sens Actuators B* 157.2 (2011), pp. 329–352.

[37] Ángela I. López-Lorente, Miguel Valcárcel, and Boris Mizaikoff. "Continuous flow synthesis and characterization of tailor-made bare gold nanoparticles for use in SERS". In: *Microchimica Acta* 181 (2014), pp. 1101–1108.

[38] Y. Imai et al. "Optically readable hydrogen sensor using Pd/Y double-layered thin films". In: *AZojomo (ISSN 1833-122X)* 2.3346 (2006). URL: DOI:10.2240/azojomo0197.

[39] Yoshiro Imura et al. "Preparation and Catalytic Activity of Pd and Bimetallic Pd–Ni Nanowires". In: *Langmuir* 30 (2014), pp. 5026–5030.

[40] Susanna Jansat et al. "A case for enantioselective allylic alkylation catalyzed by palladium nanoparticles". In: *Journal of the American Chemical Society* 126.6 (2004), pp. 1592–1593.

[41] K.J. Jeon et al. "Nanotechnology Individual Pd nanowire hydrogen sensors fabricated by electron-beam lithography". In: *Nanotechnology* 20.13 (2009), p. 135502.

[42] Kye Jin Jeon et al. "Individual Pd nanowire hydrogen sensors fabricated by electron–beam lithography". In: *Nanotechnology* 20.13 (2009), p. 135502.

[43] R.K. Joshi et al. "Pd Nanoparticles and Thin Films for Room Temperature Hydrogen Sensor". In: *Nanoscale Res Lett.* 4 (2009), p. 1191. URL: doi.org/10.1007/s11671-009-9379-6.

[44] Y w Jun, J s Choi, and J. Cheon. "Shape control of semiconductor and metal oxide nanocrystals through nonhydrolytic colloidal routes". In: *Angew Chem Int Ed Engl.* 45.21 (2006), pp. 3414–3439. URL: DOI:10.1002/anie.200503821.

[45] Babak Karimi et al. "Highly Efficient Aerobic Oxidation of Alcohols Using a Recoverable Catalyst: The Role of Mesoporous Channels of SBA-15 in Stabilizing Palladium Nanoparticles". In: *Angewandte Chemie* 29.29 (2006), pp. 4894–4897.

[46] M. Khanuja et al. "Concentration-specific hydrogen sensing behavior in monosized Pd nanoparticle layers". In: *Nanotechnology* 20 (2008), p. 015502.

[47] M. Khanuja et al. "Interaction of Hydrogen with Rare Earth and Palladium Nanoparticles: Basic Issues and Novel Devices". In: *ChemInform, Proc. Indian National Science Academy* 43.51 (2011). URL: https://doi.org/10.1002/chin.201251173.

[48] Dae-Seon Kim, Min-Su Park, and Jae-Hyung Jang. "A High-Coverage Nanoparticle Monolayer for the Fabrication of a Subwavelength Structure on InP Substrates". In: *J. Nanosci. Nanotechnol.* 11.8 (2011), pp. 7407–7411.

[49] Sang-Wook Kim et al. "Fabrication of hollow palladium spheres and their successful application to the recyclable heterogeneous catalyst for Suzuki coupling reactions". In: *Journal of the American Chemical Society* 124.26 (2002), pp. 7642–7643.

[50] A. Klinkova et al. "Shape-dependent interactions of palladium nanocrystals with hydrogen". In: *Small* 12.8 (2016), pp. 2450–2458.

[51] A. Kolmakov et al. "Enhanced Gas Sensing by Individual SnO_2 Nanowires and Nanobelts Functionalized with Pd Catalyst Particles". In: *Nano Lett.* 5.4 (2005), pp. 667–673.

[52] Min Serk Kwon et al. "Palladium nanoparticles entrapped in aluminum hydroxide: dual catalyst for alkene hydrogenation and aerobic alcohol oxidation". In: *Organic letters* 7.6 (2005), pp. 1077–1079.

[53] F.A. Lewis. *The Palladium Hydrogen System*. Academic Press, London, 1967.

[54] G. Li et al. "Shape-dependent hydrogen-storage properties in Pd nanocrystals: which does hydrogen prefer, octahedron (111) or cube (100)?" In: *J Am. Chem. Soc.* 136.29 (2014), pp. 10222–10225.

[55] Yin Li, Edna Boone, and Mostafa A El-Sayed. "Size effects of PVP-Pd nanoparticles on the catalytic Suzuki reactions in aqueous solution". In: *Langmuir* 18.12 (2002), pp. 4921–4925.

[56] M. Lischka and A. Grob. "Hydrogen on palladium: A model system for the interaction of atoms and molecules with metal surfaces". In: *Recent Developments in Vacuum Science and Technology* 37 (2003), pp. 111–132.

[57] Muhua Luo et al. "Facile removal of polyvinylpyrrolidone (PVP) adsorbates from Pt alloy nanoparticles". In: *J. Mater. Chem. A* 3 (2015), pp. 2770–2775. URL: https://doi.org/10.1039/C4TA05250A.

[58] Radha Narayanan and Mostafa A. El-Sayed. "Effect of colloidal catalysis on the nanoparticle size distribution: Dendrimer – Pd vs PVP – Pd nanoparticles catalyzing the Suzuki coupling reaction". In: *The Journal of Chemistry B* 108.25 (2004), pp. 8572–8580.

[59] Radha Narayanan and Mostafa A. El-Sayed. "Effect of colloidal nanocatalysis on the metallic nanoparticle shape: the Suzuki reaction". In: *Langmuir* 21.5 (2005), pp. 2027–2033.

[60] Radha Narayanan and Mostafa A. El-Sayed. "Shape-dependent catalytic activity of platinum nanoparticles in colloidal solution". In: *Nano letters* 4.7 (2004), pp. 1343–1348.

[61] Mahmoud Goodarz Naseri, Elias Saion, and Nasrin Khalil Zadeh. "The amazing effects and role of PVP on the crystallinity, phase composition and morphology of nickel ferrite nanoparticles prepared by thermal treatment method". In: *International Nano Letters* 3.1 (2013), p. 19.

[62] Colleen L. Nehl, Hongwei Liao, and Jason H. Hafner. "Optical Properties of Star-Shaped Gold Nanoparticles". In: *Nano Lett.* 6.4 (2006), pp. 683–688.

[63] Abderrafik Nemamcha, Jean-Luc Rehspringer, and Djameledine Khatmi. "Synthesis of palladium nanoparticles by sonochemical reduction of palladium(II) nitrate in aqueous solution". In: *J Phys Chem B* 110 (2006), pp. 383–7. URL: doi:10.1021/jp0535801..

[64] J-S Noh, J.M Lee, and W. Lee. "Low-Dimensional Palladium Nanostructures for Fast and Reliable Hydrogen Gas Detection". In: *Sensors* 11.1 (2011), pp. 825–851.

[65] J-S Noh, J.M Lee, and W Lee. "Low-Dimensional Palladium Nanostructures for Fast and Reliable Hydrogen Gas Detection". In: *Sensors* 11.1 (2011), pp. 825–851.

[66] Katherine L. Orchard, Milo S. P. Shaffer, and Charlotte K. Williams. "Organometallic Route to Surface-Modified ZnO Nanoparticles Suitable for In Situ Nanocomposite Synthesis: Bound Carboxylate Stoichiometry Controls Particle Size or Surface Coverage". In: *Chem. Mater.* 24.13 (2012), pp. 2443–2448.

[67] J.Y. Park et al. "Surface-area-controlled synthesis of porous TiO_2 thin films for gas-sensing applications". In: *Nanotechnology* 28.9 (2017), p. 095502. URL: https://doi.org/10.1088/1361-6528/aa5836.

[68] Frederic Paul, Joe Patt, and John F. Hartwig. "Palladium-catalyzed formation of carbon-nitrogen bonds. Reaction intermediates and catalyst improvements in the hetero cross-coupling of aryl halides and tin amides". In: *Journal of the American Chemical Society* 116.13 (1994), pp. 5969–5970.

[69] D-T Phan and G-S Chung. "Reliability of hydrogen sensing based on bimetallic Ni–Pd/graphene composites". In: *Int J Hydrogen Energy* 39.35 (2014), pp. 20294–20304.

[70] D-T Phan and G-S Chung. "Reliability of hydrogen sensing based on bimetallic Ni–Pd/graphene composites". In: *Int J Hydrogen Energy* 39.35 (2014), pp. 20294–20304.

[71] Pooja, P.B. Barman, and S.K. Hazra. "Role of Capping Agent in Palladium Nanoparticle Based Hydrogen Sensor". In: *J Clust Sci* 29 (2018), pp. 1209–1216. URL: https://doi.org/10.1007/s10876-018-1438-7.

[72] J.M. Rahm and P. Erhart. "Beyond magic numbers: atomic scale equilibrium nanoparticle shapes for any size". In: *Nano Lett.* 17.9 (2017), pp. 5775–5781.

[73] R. Ramachandran and R.K. Menon. "An overview of industrial uses of hydrogen". In: *Int J Hydrogen Energy* 23.7 (1998), pp. 593–598.

[74] Manfred T. Reetz and Elke Westermann. "Phosphane-free palladium-catalyzed coupling reactions: the decisive role of Pd nanoparticles". In: *Angewandte Chemie International Edition* 39.1 (2000), pp. 165–168.

[75] Bedabrata Saha, Toon H. Evers, and Menno W. J. Prins. "How Antibody Surface Coverage on Nanoparticles Determines the Activity and Kinetics of Antigen Capturing for Biosensing". In: *Anal. Chem. 2014, 86, 16, 8158–8166* 86.16 (2014), pp. 8158–8166.

[76] S. Sawoo et al. "Size controlled synthesis of Pd nanoparticles in water and their catalytic application in C-C coupling reactions". In: *Tetrahedron* 65.22 (2009), pp. 4367–4374.

[77] Qingming Shen et al. "Morphology-controlled synthesis of palladium nanostructures by sonoelectrochemical method and their application in direct alcohol oxidation". In: *The Journal of Physical Chemistry C* 113.4 (2009), pp. 1267–1273.

[78] Ali R. Siamaki et al. "Microwave-assisted synthesis of palladium nanoparticles supported on graphene: A highly active and recyclable catalyst for carbon–carbon cross-coupling reactions". In: *Journal of catalysis* 279.1 (2011), pp. 1–11.

[79] H. Song et al. "Pt nanocrystals: shape control and Langmuir-Blodgett monolayer formation". In: *J Phys Chem B* 109.1 (2005), pp. 188–193. URL: doi:10.1021/jp0464775.

[80] Peter Strasser et al. "Lattice-strain control of the activity in dealloyed core-shell fuel cell catalysts". In: *Nature Chem* 2 (2010), pp. 454–460. URL: https://doi.org/10.1038/nchem.623.

[81] Y. Sun and Y. Xia. "Shape-Controlled Synthesis of Gold and Silver Nanoparticles". In: *Science* 298.5601 (2002), pp. 2176–2179. URL: DOI:10.1126/science.1077229.

[82] Chong Sook Paik Sung, Eumi Pyun, and Han Li Sun. "Characterization of epoxy cure by UV-visible and fluorescence spectroscopy: azo chromophoric labeling approach". In: *Macromolecules* 19.12 (1986), pp. 2922–2932.

[83] Mario Tagliazucchi et al. "Optical properties of responsive hybrid Au@ polymer nanoparticles". In: *ACS Nano* 6.9 (2012), pp. 8397–8406. URL: doi:10.1021/nn303221y.

[84] A. Tao, P. Sinsermsuksakul, and P. Yang. "Polyhedral Silver Nanocrystals with Distinct Scattering Signatures". In: *Angew Chem Int Ed* 45.28 (2006), pp. 4597–4601.

[85] A.R. Tao, S. Habas, and P. Yang. "Shape Control of Colloidal Metal Nanocrystals". In: *Small* 4.3 (2008), pp. 310–325.

[86] Jing Teng et al. "Effect of water vapor sorption on local structure of poly (vinylpyrrolidone)". In: *J Pharm Sci* 99.9 (2010), pp. 3815–3825.

[87] Prashant Thakur et al. "Structural and optical properties of $Mn_{0.5}Zn_{0.5}Fe_2O_4$ nano ferrites: Effect of sintering temperature". In: *Materials Chemistry and Physics* 193 (2017), pp. 285–289. URL: https://doi.org/10.1016/j.matchemphys.2017.02.043.

[88] Ph. Toneguzzo et al. "CoNi and FeCoNi fine particles prepared by the polyol process: Physicochemical characterization and dynamic magnetic properties". In: *Journal of Materials Science* 35.15 (2000), pp. 3767–3784.

[89] Sunil Walia et al. "Transparent Pd Wire Network-Based Areal Hydrogen Sensor with Inherent Joule Heater". In: *ACS Appl. Mater. Interfaces* 8.35 (2016), pp. 23419–23424.

[90] D.M. Wells et al. "Metastability of the atomic structures of size-selected gold nanoparticles". In: *Nanoscale* 7 (2015), pp. 6498–6503.

[91] B. Wiley et al. "Polyol Synthesis of Silver Nanoparticles-Use of Chloride and Oxygen to Promote the Formation of Single-Crystal Truncated Cubes and Tetrahedrons". In: *Nano Lett* 4.9 (2004), pp. 1733–1739.

[92] B. Wiley et al. "Shape-Controlled Synthesis of Metal Nanostructures: The Case of Silver". In: *Chem Eur J* 11 (2005), pp. 454–463.

[93] G.K Williamson and W.H Hall. "X-ray line broadening from filed aluminium and wolfram". In: *Acta Metallurgica* 1.1 (1953), pp. 22–31. URL: https://doi.org/10.1016/0001-6160(53)90006-6.

[94] Y. Xiong et al. "Synthesis and Mechanistic Study of Palladium Nanobars and Nanorods". In: *J Am Chem Soc* 129.12 (2007), pp. 3665–3675.

[95] Yujie Xiong et al. "Size-Dependence of Surface Plasmon Resonance and Oxidation for Pd Nanocubes Synthesized via a Seed Etching Process". In: *Nano Lett.* 5.7 (2005), pp. 1237–1242.

[96] Noboru Yamazoe, Go Sakai, and Kengo Shimanoe. “Oxide semiconductor gas sensors”. In: *Catalysis Surveys from Asia* 7.1 (2003), pp. 63–75.

[97] Di Yang et al. “An integrated experimental and theoretical study on the optical properties of uniform hairy noble metal nanoparticles”. In: *Nanoscale* 10.48 (2018), pp. 22750–22757.

[98] Xuemei Zhang et al. “Shape-controlled synthesis of Pt nanopeanuts”. In: *Scientific reports* 6 (2016), p. 31404.

[99] Xuemei Zhang et al. “Shape-controlled synthesis of Pt nanopeanuts”. In: *Scientific reports* 6 (2016), p. 31404.